EXPERIMENTAL EVALUATION OF SILICON EXPANSION VALVE TECHNOLOGY

A Thesis

by

KAIMI GAO

Submitted to the Office of Graduate and Professional Studies of
Texas A&M University
in partial fulfillment of the requirements for the degree of

MASTER OF SCIENCE

Chair of Committee,	Bryan Rasmussen
Committee Members,	Kalyan Annamalai
	Garng Huang
Head of Department,	Andreas Polycarpou

August 2015

Major Subject: Mechanical Engineering

ABSTRACT

Residential and commercial buildings consume 40% of the energy used in the United States. Heating and cooling uses more energy than any other system in a building. Typically, 43% of a building utility bill goes to HVAC equipment. By combining proper equipment maintenance and upgrades with appropriate insulation, air sealing, and thermostat settings, energy usage can be cut from 20% to 50%. In this research, advanced valves and control algorithms are studied to improve the efficiency and reduce the energy consumption of vapor compression air conditioning and refrigeration systems. The characteristics of the new generation of MEMS based flow control devices have been tested on single and multi-evaporator systems. This research conducted a comprehensive set of experimental tests that identify the most effective elements of an advanced valve control strategy under a variety of operating conditions. The performance of the new MEMS actuators with different control strategies is compared with the standard mechanical valves and a commercially available superheat controller. Preliminary research results reveal efficiency gains with a cascaded control algorithm over both the thermal expansion valves and the commercial superheat controller.

DEDICATION

To my family and friends.

ACKNOWLEDGEMENTS

I would link to acknowledge DunAn Microstaq for financial support to this research work. I would like to thank my advisor, Dr. Rasmussen for his continuous assistance and guidance throughout my study and research. I would also like to thank my committee members, Dr. Kalyan Annamalai, Dr. Garng Huang for serving on my thesis committee.

Thanks also go to my friends and colleagues at Thermo-Fluid Control Laboratory: Chao Wang, Erik Rodriguez, Chris Price, Chris Bay, Trevor Terrill, Rawand Jalal, Edwin Youmi, Priyam Parikh and Shuangshuang Liang for their help and advice. I would like to thank the department faculty and staff for making my time at Texas A&M University a great experience.

Finally, thanks to my mother and father for their support and encouragement.

ABBREVIATIONS

VCC	Vapor Compression Cycle
HVAC&R	Heating, Ventilation, Air Conditioning and Refrigeration
AEV	Automatic Expansion Valve
TXV	Thermal Expansion Valve
EEV	Electrical Expansion Valve
PDA	Direct Acting Silicon Expansion Valve
MSEV	Modular Silicon Expansion Valve
USHC	Universal Superheat Controller
DMQ	DunAn Microstaq
MEMS	Micro-electrical-mechanical System

NOMENCLATURE

	Units	**Explanation**
P_e	[kPa]	Evaporator Pressure
P_c	[kPa]	Condenser Pressure
$\dot{m}$	[kg/s]	Refrigerant Mass Flow Rate
Q	[W] or [kW]	Cooling Capacity
Q_{ave}	[W] or [kW]	Average Cooling Per Cycle
T_{SH}	[°C]	Superheat

TABLE OF CONTENTS

Page

LIST OF FIGURES

Page

LIST OF TABLES

Page

CHAPTER I

INTRODUCTION AND LITERATURE REVIEW

1.1 Background

Nearly 40% of total U.S. energy consumption in 2011 was consumed in residential and commercial buildings, or about 40 quadrillion British thermal units, as found in the US building energy data book [1]. Heating and cooling systems use more energy than any other system in a building. Typically, 43% of a building utility bill goes to HVAC equipment 0. By combining proper equipment maintenance and upgrades with appropriate insulation, air sealing, and thermostat settings, energy usage can be cut from 20% to 50% [1]. Supermarkets are one of the most energy-intensive types of commercial buildings. Significant electrical energy is used to maintain chilled and frozen food in both product display cases and walk-in storage coolers as shown in Figure 1. They have a wide range of sizes and range in size from less than 10,000 sq. ft. to greater than 70,000 sq. ft. total selling area [2]. A typical supermarket consumes roughly 2 million kWh annually, and roughly half is for refrigeration [2]. Therefore any improvement in the energy efficiency of the supermarket refrigeration system will directly affect the store's profit margin.

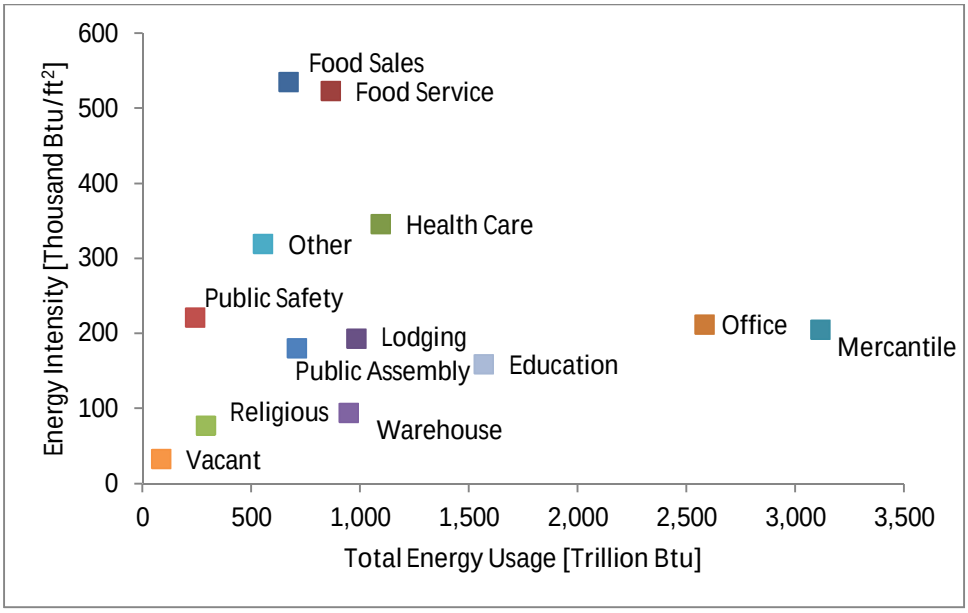

Figure 1: Energy Intensity 2002 [3]

Vapor compression is the most common technology for residential, commercial and industrial air conditioning and refrigeration. The vapor-compression cycles uses a circulating refrigerant as the medium which absorbs and removes energy from the space to be cooled and subsequently rejects that energy elsewhere. An ideal vapor compression cycle is shown in Figure 2.

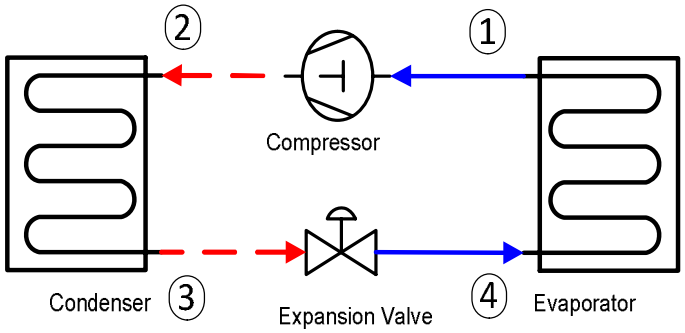

Figure 2: Ideal Vapor Compression Cycle [3]

Compressor, condenser, expansion valve and evaporator are the basic components for a vapor compression cycle. An ideal vapor compression cycle involves four processes: 1) isentropic compression in a compressor, 2) isobaric heat rejection in a condenser, 3) isenthalpic expansion in an expansion valve, 4) isobaric heat absorption in an evaporator. The p-h diagram of a vapor compression system is shown in Figure 3. The first step of the thermodynamic cycle starts in the compressor. It turns the low pressure, gaseous refrigerant into a high pressure, high temperature gas by adding energy to the refrigerant (process 1 to 2). Then the refrigerant goes into the condenser, where heat exchange happens here with the secondary fluid (usually water or air). Heat is rejected to the secondary fluid as the refrigerant condenses into a high pressure liquid (process 2 to 3). Safety equipment usually placed after condenser to ensure that the refrigerant is in saturation liquid condition before entering the valve. Isenthalpic valve throttling happens in process 3 to 4 where the saturated liquid refrigerant enters an expansion valve, and expands to a low-pressure, low temperature, two-phase fluid. As the two-phase fluid passes through the evaporator, heat energy is absorbed from the zone

as the refrigerant boils. The refrigerant evaporates into a low pressure superheated vapor when leaving the evaporator. The cycle restarts again with the compressor. In process 4 to 1, the degree of superheat is a crucial factor for safe compressor operation. Superheat is defined as temperature difference between the evaporator outlet temperature and saturation temperature of the evaporator pressure.

$$T_{SH} = T_{outlet} - T_{saturation}$$

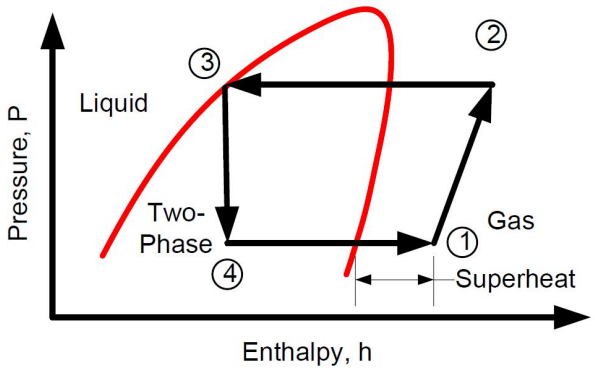

Figure 3: P-h Diagram of a Vapor Compression System [3]

1.2 Literature Review

Expansion valves are a primary means of metering refrigerant flow in vapor compression system. Orifice and capillary valves have fixed throttling area, and are designed to meter the proper flow of refrigerant at a particular operation condition. More complex valves utilize mechanical or electronic means to regulate refrigerant flow based on pressure or temperature measurements. The capillary valve is a copper tube with very small internal diameter. The small diameter and long length make the capillary valve a

good choice as throttling device when using in certain ambient conditions with simple superheat requirements. Thermostatic expansion valves (TXV) utilize a sensing bulb filled with a two-phase refrigerant placed at the evaporator outlet to measure superheat temperature. As the refrigerant temperature at the evaporator outlet increases, the pressure of the two-phase fluid in the sensing bulb also increases. The bulb pressure acts on a diaphragm inside the bulb to increase/decrease the flow area accordingly. Automatic expansion valves (AEV) alter the flow area to regulate pressure, rather than superheat. Electrical expansion valves (EEV) modify the flow area using an externally controlled mechanism, usually using a stepper motor [5], based on the electrical signals from separate sensors measuring evaporator superheat.

Elliott and Rasmussen [6] proposed a hybrid valve approach, using both mechanical and electrical feedback. The proposed valve is shown to provide transient performance superior to typical mechanical valves during start up or transient disturbance conditions, to more robust to large changes in operating conditions than typical mechanical valves and more robust to motor failure than purely electronic valves and have longer installed use before failure. Figure 4 shows the development of expansion valve over time.

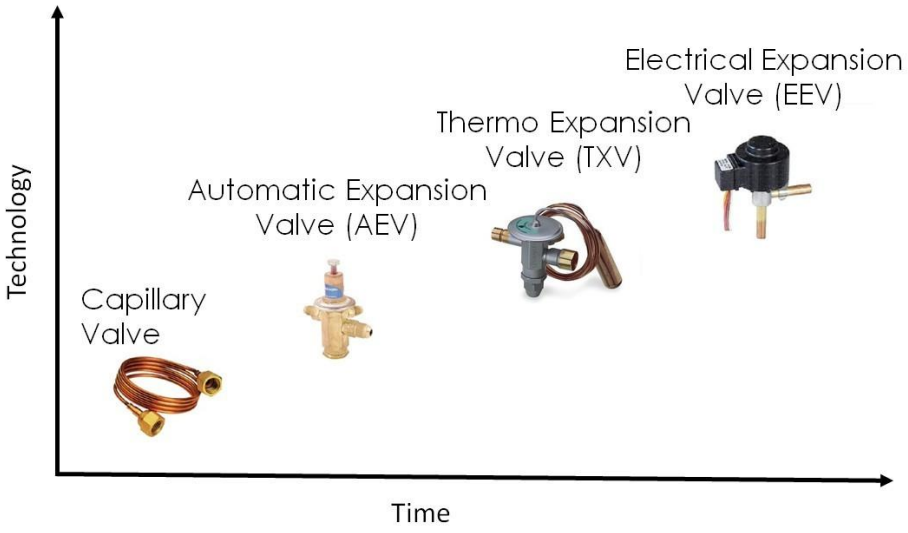

Figure 4: Valve Development

MEMS (micro-electro-mechanical systems) have been used for a variety of applications in metering liquids and gases (microfluidics) [7], due to their increased performance, small size and high reliability. The application of MEMS based microvalves in refrigeration has been discussed that the main challenge for thermally activated microvalves was the refrigerant's thermodynamic state [7]. Because the refrigerant was prepared to be on the edge of flashing just after the valve or just prior to entering the system evaporator and so little or no heat was allowed to be removed from the microvalve by refrigerant [7]. The solution to this problem, Henning added a second hollow Pyrex layer between the capping Pyrex layer and the membrane layer allowing little heat to be removed [7]. The hollowed layer was filled with FC liquid [7]. It isolated the membrane thermally from the heater resistor due to the lowest thermal conductivity in the microvalve of the Fluorinert^{TM} (FC) liquid [7].

Recently DunAn Microstaq developed a silicon servo valve, a semiconductor microfluidic MEMS microvalve that can be incorporated in any flow control related application or system [8]. The advantages like reduced size and weight, better structural reliability, and simplified operational use make the MEMS microvalves popular in the area of automotive transmission, air conditioning and refrigeration [8]. DMQ's patented silQflo® is a specialized semiconductor based microvalve composed of three bonded silicon wafers [8]. It operates using thermal actuator principles to adjust the degree of opening of the valve orifice. Capable of sensing flows at the microfluidic level, the silQflo® Silicon Servo Valve can be used as is, individually, or utilized in conjunction as part of a larger flow control valve, such as the Modular Silicon Expansion Valve (MSEV) or Mobile Expansion Valve (MEV) [8].

Figure 5: DMQ's silQflo [8]

Figure 6: DMQ's MSEV [8]

In the MSEV, the silQflo® Silicon Servo Valve is used in conjunction with a spool valve to create a device capable of amplifying micro scale flow to a macro scale [8]. The size of the silQflo® Silicon Servo Valve is shown in Figure 5. Figure 6 is an example of DMQ's Modular Silicon Expansion Valve. Using a closed loop feedback system based on pressure differentials between the valve and overall system, the MSEV is designed for superheat fluid control in air conditioning and refrigeration systems [8]. A Universal Superheat Controller or Sensor (USHX) as seen in Figure 7 is available to use with the MSEV, to control the refrigerant flow to the designed level to meet the system condition [8].

Figure 7: DMQ's Universal Superheat Controller (USHX) [8]

Silicon expansion valves have many advantages over conventional expansion valves. K. Higuchi et al [9] and later Mithraratne et al [10] investigated the dynamic behavior of thermostatic expansion valves both experimentally and numerically. Mithraratne and Wijeysundera revealed the existence of hysteresis to explain the failure of linear model of the thermal expansion valve and the distributed model of evaporators to reproduce the valve hunting behavior that occurs in practice. N.J. Hewitt et al [11] carried out on an extensive study to compare the performances of thermostatic expansion valves, thermoelectric expansion valves, solenoid expansion valves and motorized types of expansion valves. While electronic expansion valves provided better superheat control than thermostatic expansion valves at transient conditions, they still did not provide an ideal solution to the problem. Electronic expansion valves were found to be generally complex, expensive and fragile.

In an earlier project with DMQ, a detailed evaluation between different types of expansion valves was made.

Traditional expansion valves such as orifice valves or capillary tubes do not have any type of feedback mechanism to regulate the refrigerant fluid flow. As a result, there is a distinct risk of starving the evaporator resulting in reduced cooling capacity, or flooding the evaporator and potentially harming the compressor [12].

Thermostatic expansion valves (TXV) directly alter the valve area proportional to regulate superheat. Due to the heat conduction through pipes and TXV sensing bulb, there is a time lag in this process. Valve hunting is commonly happening in the TXV used systems [13]. It is generally avoided by sacrificing efficiency and selecting a higher superheat setpoint.

Electronic expansion valves utilize step motors to control the valve position. The use of step motors enables the use of more advanced control algorithms that can avoid these undesirable behaviors.

Previous studies effectively illustrated that TXV controlled systems were less sensitive to over/under-charged conditions than fixed orifice devices [14]. This has been shown for EEVs as well [15]. Although a direct comparison of charge sensitivity for TXV and EEV controlled systems was not found, as a more flexible device, the EEV would presumably be more robust to changes in refrigerant charge.

The expansion valve has a direct impact on efficiency, as it meters the refrigerant flow through the evaporator. Although the cooling capacity is maximized when the

evaporator is filled with two-phase fluid, optimal system efficiency if generally obtained with a few degrees of evaporator superheat.

In some previous work by X. He and S. Liu [16], gain scheduling has been proven to be a way to handle nonlinearities in refrigeration systems using multi-input multi-output control method. L. S. Larsen [17] proposed an approach that a suboptimal condenser pressure was found in order to minimize the energy consumption without changing the cooling capacity. Further study of this approach can be applied to a system which has a capacity and a superheat control without altering these control loops. C. Tian and C. Dou [18] found refrigeration system with variable speed compressor where the compressor and the expansion valve are controlled by two independent loops the effect of cross coupling between the loops may cause instability or unacceptable performance. Then a new control strategy where the superheat temperature is controlled by the compressor and the cooling capacity by the refrigerant mass flow is compared to a conventional control strategy based on a thermostatic expansion valve for control on superheat in [19] and [20]. Compared to method proposed in [16], no gain scheduling of superheat controller is necessary to cover a big region of operation. M.S. Elliott and B.P. Rasmussen 0 proposed a cascaded superheat control algorithm that eliminates most of the nonlinearity of the response between algorithm-generated control input and the superheat output, while only requiring pressure and temperature measurements. The approach was implemented using both an EEV and a HEV. HEV using mechanical pressure regulator functions more quickly and using EEV enables reduction of nonlinearities. A. Gupta [21] applied a cascaded controller for a multi-evaporator

refrigeration system. His work presents a design of an effective cascaded controller on MEMS based Silicon Expansion Valves. The experiments conducted on the supermarket refrigeration system indicate significant energy saving using SEV compared with TXV. The energy savings is attributed to the fact that the compressor run time is less for the DMQ commercial controller and the cascaded controller. But in his study, he didn't look into the most effective elements of an advanced valve control strategy under a variety of operating conditions. Shafiei [21] proposed a decentralized control method to govern the electrical power consumption of supermarket refrigeration systems for demand-side management in the smart gird. A decentralized model predictive control was proposed to be used for a multi-evaporator air conditioning system by M. S. Elliott and B. P. Rasmussen [23]. The control algorithm is a flexible, two level structure that uses predictive control methods at both levels to achieve the goals of each controller. The proposed method succeeded in achieving desired temperatures of different zones serviced by the same vapor compression cycles while maxing energy efficiency in the process. Future opportunities to improve the implementation of the control architecture are the efficiency of the system is dependent upon the cooling zone temperature.

1.3 Research Objective and Tasks

The research was divided into two parts.

Part 1: DunAn Microstaq (DMQ) currently produces direct acting silicon expansion valves (PDA) and piloted expansion valves. The new generation PDA valves should have repeatable operation behavior and have the capability to handle advanced

control strategies. Small internal leakage rates and small cooling capacities of the PDAs give them unique characteristics. In this part of research, the characteristics of the new generation PDAs will be experimentally examined. The valves will be installed on a multi-evaporator system, in parallel with current expansion valves. The existing experimental equipment will be modified for the tests.

Part 2: The characteristics of silicon expansion valves make them a good choice as an advanced throttling device in the refrigeration systems. In this part of research, DMQ's modular silicon expansion valves (MSEV) will be installed on a multi-evaporator Hussman commercial refrigeration system. A comprehensive set of experimental tests that will identify the most effective elements of an advanced valve control strategy under a variety of operating conditions.

1.4 Thesis Organization

This thesis is organized as follows: Chapter 2 introduces the experimental systems used for the research. It also includes details about the sensors and data acquisition systems. In Chapter 3, the testing method and the test results of the leak rate test are shown in detail. Chapter 4 describes the test principles and experimental results of the cooling capacity tests. Chapter 5 quantifies efficiency gains using advanced control algorithms with MSEV. Final discussion, conclusion and future work are provided in chapter 6.

CHAPTER II

EXPERIMENTAL SYSTEMS

2.1 Multi-evaporator Water Chiller System

The experimental system used for the tests presented in Chapter 3 is a custom-built, small-scale three-evaporator water chiller system. It uses refrigerant R134a as the working fluid. A liquid receiver is installed at the end of the condenser to ensure that saturated liquid is fed to the expansion valves. There is a bypass manifold for the receiver so that tests with refrigerant subcooling can be conducted if desired. Manual shutoff valves are used throughout the system to reconfigure the refrigerant flow as desired. These valves give the system the ability to be partially turned on. The compressor on the system is a variable speed brushless DC compressor. Figure 8 is the photo of the system. Figure 9 is a schematic structure of the refrigerant cycle of the system.

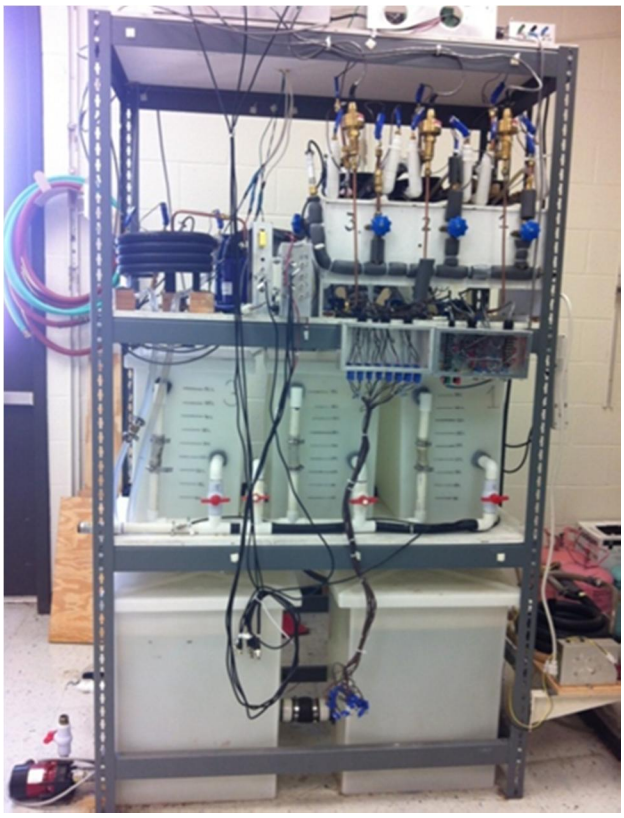

Figure 8: Water Chiller System

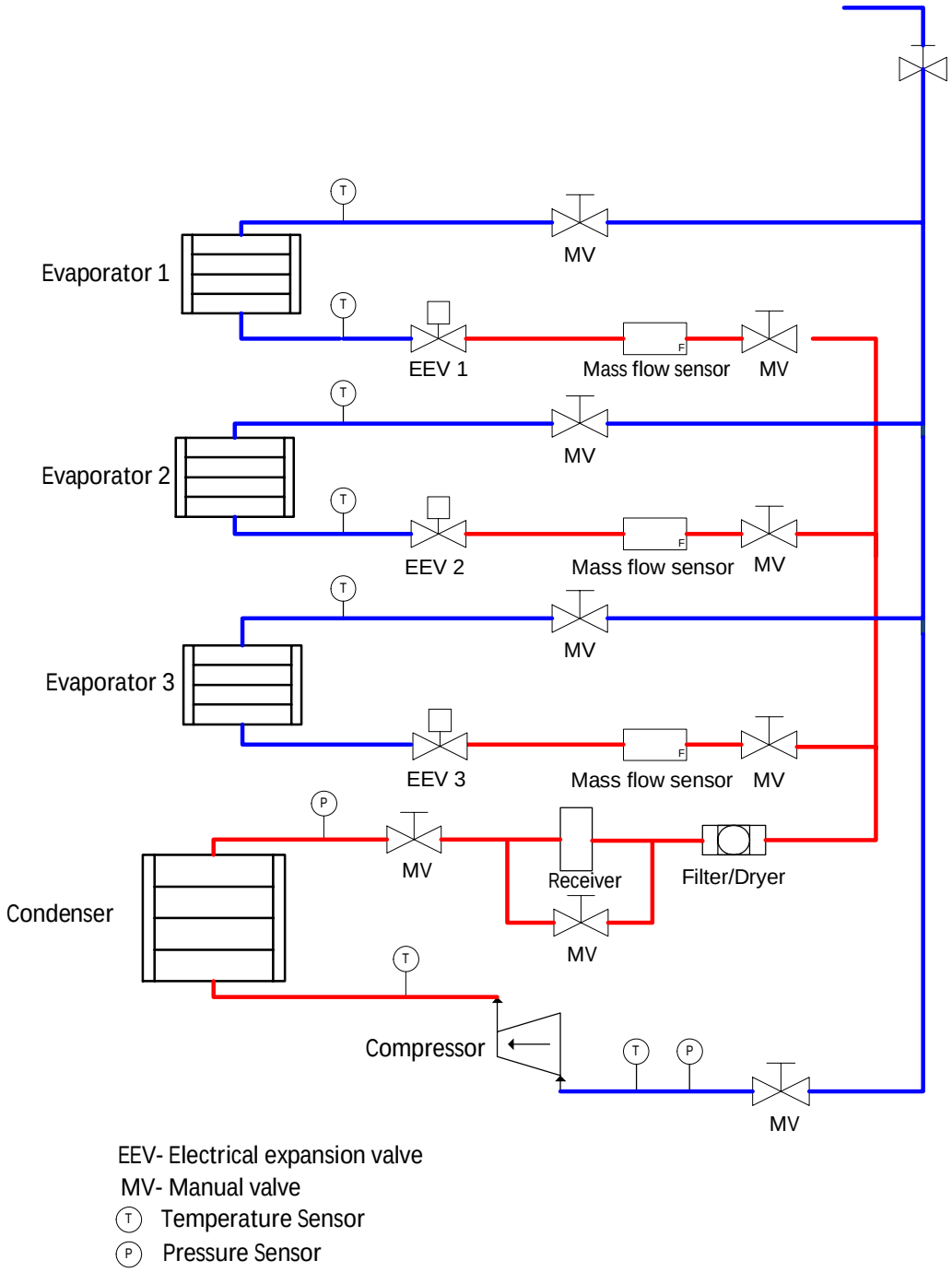

Figure 9: Schematic of the Refrigerant Cycle of the System

Water is used as the secondary fluid in the heat exchangers. Three tanks of water are pumped by three separate pumps to provided heat loads. Each of them contains 50 liters of water. Another tank with 260 liters of water serves as the heat sink and water in this tank is fed to the condenser. An extra heat exchanger was connected to the building chilled water to remove the thermal energy to maintain the condenser water temperature at a constant level. Figure 10 is a schematic structure of the water cycle of the system.

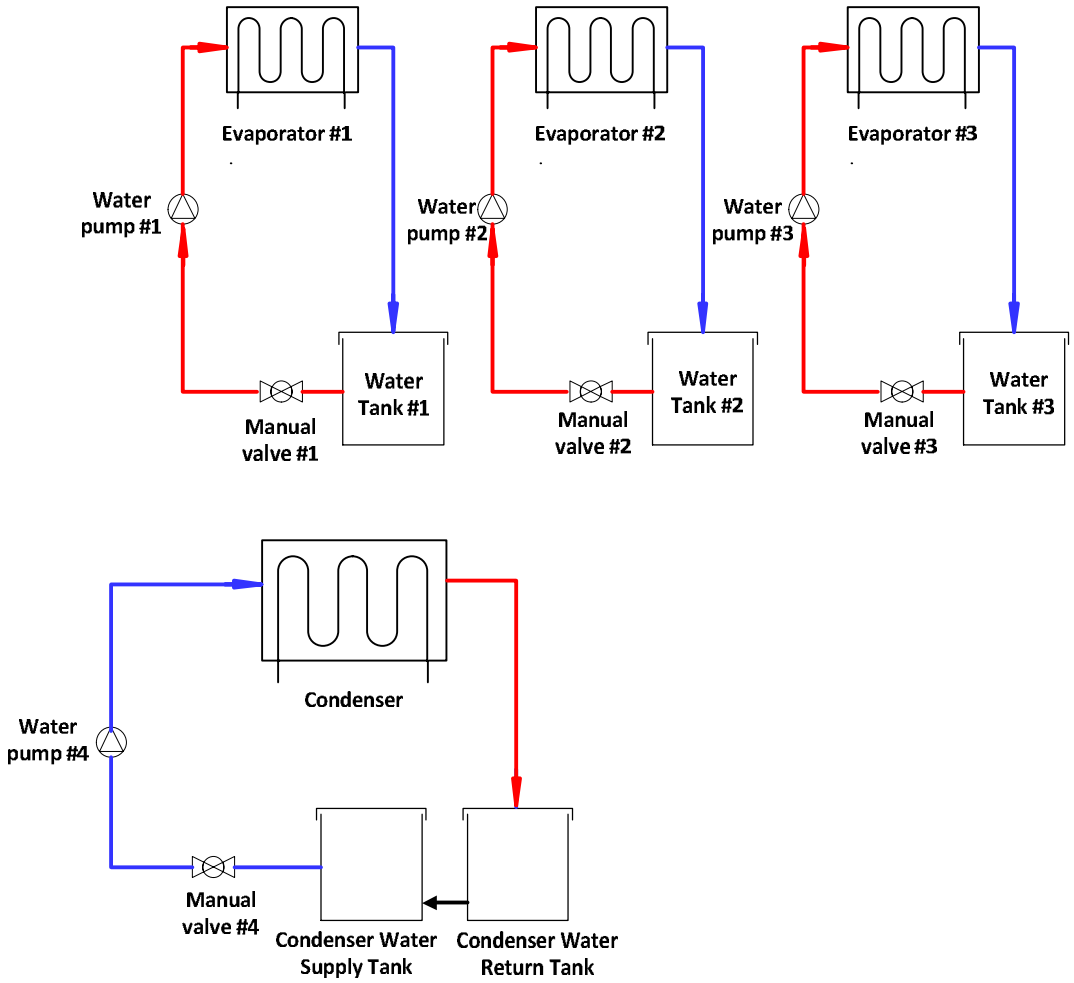

Figure 10: Schematic of the Water Cycle of the System

2.1.1 Major Components

Heat Exchanger

Four heat exchangers are installed on the water chiller system. One is condenser, the other three are evaporators. These all shell-in-tube style heat exchangers are manufactured by Packless Industries. The condenser has 1.5 tons of cooling capacity and the three evaporators are rated 0.5 ton each. Figure 11 shows one heat exchanger (condenser).

Figure 11: Heat Exchanger

Compressor

The compressor is manufactured by Masterflux. It is a scroll-type compressor with 1800 to 6500 variable speed. It operates on 48 Volts DC power supply with R-134a refrigerant. The total cooling capacity of the compressor is rated at 1.5 tons. The compressor speed is controlled by a control board from the manufacture. An extra switch is added to get the ability to manually turn the power on and off. Figure 12 is a photo of the compressor.

Figure 12: Masterflux Sierra Compressor

Expansion Valves

Three expansion valves have been installed on the system. They are electrical expansion valves (EEV) manufactured by Sporlan as shown in Figure 13.

Figure 13: Electrical Expansion Valves (EEV) Manufactured by Sporlan

2.1.2 Sensors

12 T-type thermocouples are used on the system. They are immersed in the fluid to measure the temperature at different points across the system. Swagelok tube fittings are used to install the thermocouples to the system. The thermocouples are connected to a PCI thermocouple board on the computer.

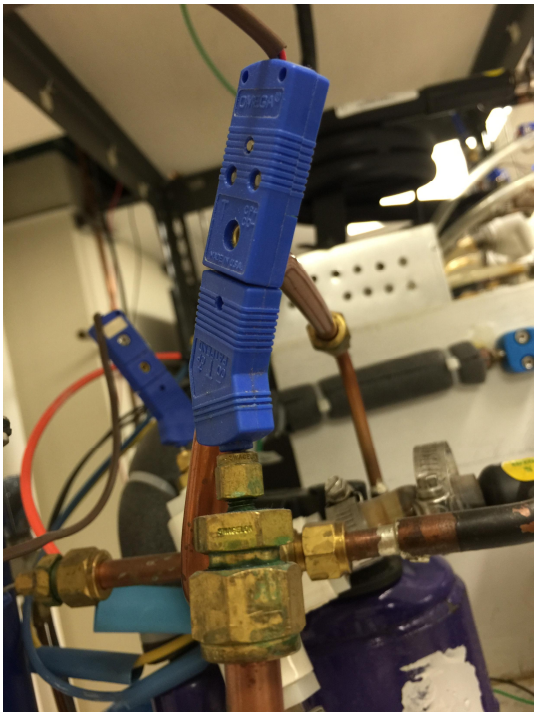

Figure 14: Type T Thermocouple

Two sealed stainless steel diaphragm-type pressure transducers manufactured by Cole-Parmer are used on the system to measure evaporator pressure and condenser pressure. One pressure transducer is installed at the outlet of the condenser which has a maximum pressure of 300 psi. The other pressure transducer with an operating range of 0-100 psi is installed to measure the evaporator pressure. All the pressure transducers have 1-5 Volts output. The output signal is connected to data acquisition boards.

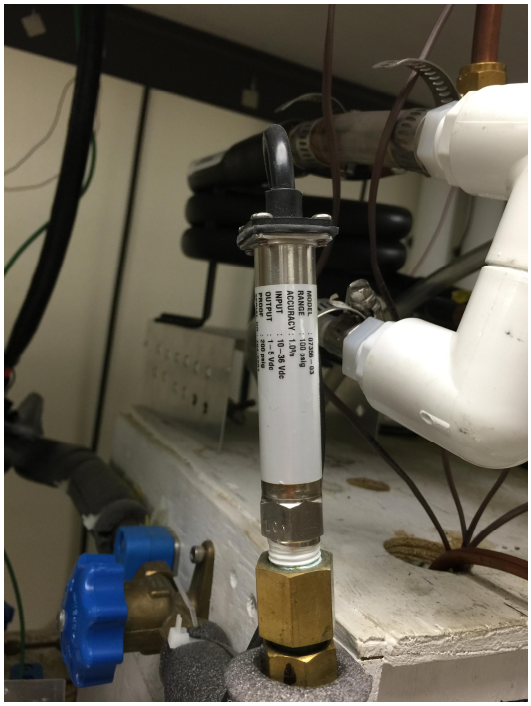

Figure 15: Pressure Transducer

Three mass flow meters are to measure refrigerant flow. They are volumetric turbine-style flow-meters manufactured by McMillan. These mass flow meters have 0-5 Volts output signal, which is connected directly into the data acquisition boards. Photo of a refrigerant mass flow meter is shown in Figure 16. All the main components of the water chiller system are shown in Table 1.

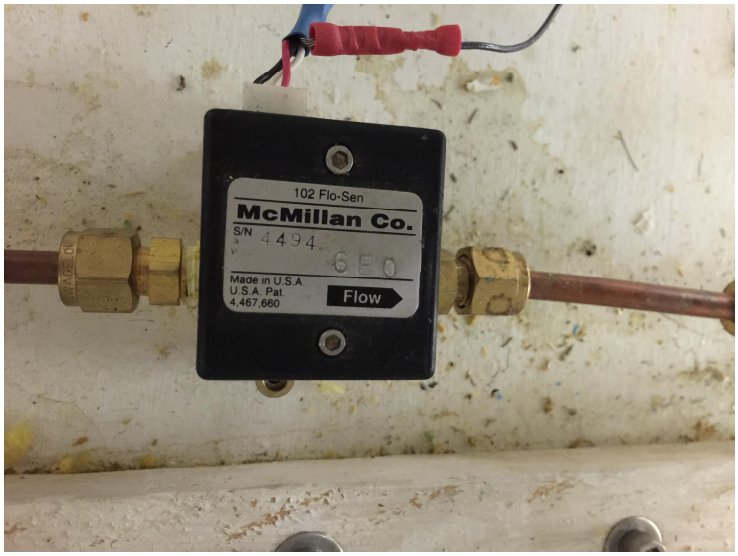

Figure 16: McMillan Mass Flow Meter

Table 1: **Main Components of Water Chiller System**

Component	Quantity	Manufacturer	Model Number
EEV	3	Sporlan	SEI 0.5-10-S
Compressor	1	Masterflux	Sierra 0.-0982Y3
Thermocouple	12	Omega	GTMQSS-062U-6
Mass Flow Meter	3	McMillan	102 Range 5
Pressure Transducer	2	Cole-Parmer	07356-04
DAQ Software	1	Quanser	WinCon 5.0

2.2 Hussman Commercial Refrigeration Unit

A Hussman commercial refrigerantion system Excel B3XC-LEP is used for the experimental tests in Chapter 4. The system is a three evaporator supermarket open door display cabinet as shown in Figure 17. A shield covering was added to the system to prevent heat transfer from the environment.

The system has three evaporators and a single constant speed compressor. The condenser is connected at the outlet of the compressor with a liquid receiver. The system uses refrigerant R404 as the working fluid. The evaporators are air cooled, finned tube heat exchangers. The condenser is a water-cooled, plate type heat exchanger. The condenser is connected to the building chilled water supply. Both the Modular Silicon Expansion Valves (MSEV) and the Thermal Expansion Valves (TXV) are installed on the system as the throttling devices. By-pass valves are used to switch between MSEVs and TXVs. Refrigerant mass flow rate are measured using three McMillan volumetric mass flow meters installed at the inlet of the evaporators. Total four pressure transducers are installed on the system, one at the outlet of the liquid receiver to measure the high side pressure and three at the outlet of each evaporator to measure the low side pressures. 11 thermocouples are used on the system at various positions to measure the refrigerant temperatures and air temperature. Three commercial DunAn Microstaq Superheat Controllers are installed at the outlet of each evaporator. The system is fitted with a smart fan control box that can change air flow rate across the fans. A schematic of the system is shown in Figure 18.

A vinyl shield covering was added to system. Velcro straps were used on the sides to seal the shield covering. The shield covering has a rolling system to raise and secure itself to any positions. The shield covering insulated the system from the ambient and helped the system to achieve the desired thermostat temperature faster. Partially open the shield covering to the ambient can simulate the system with variable loads

conditions. For the tests discussed later, the shield covering was set to a fixed position to ensure same load condition.

Figure 17: Hussman Commercial Refrigeration Unit

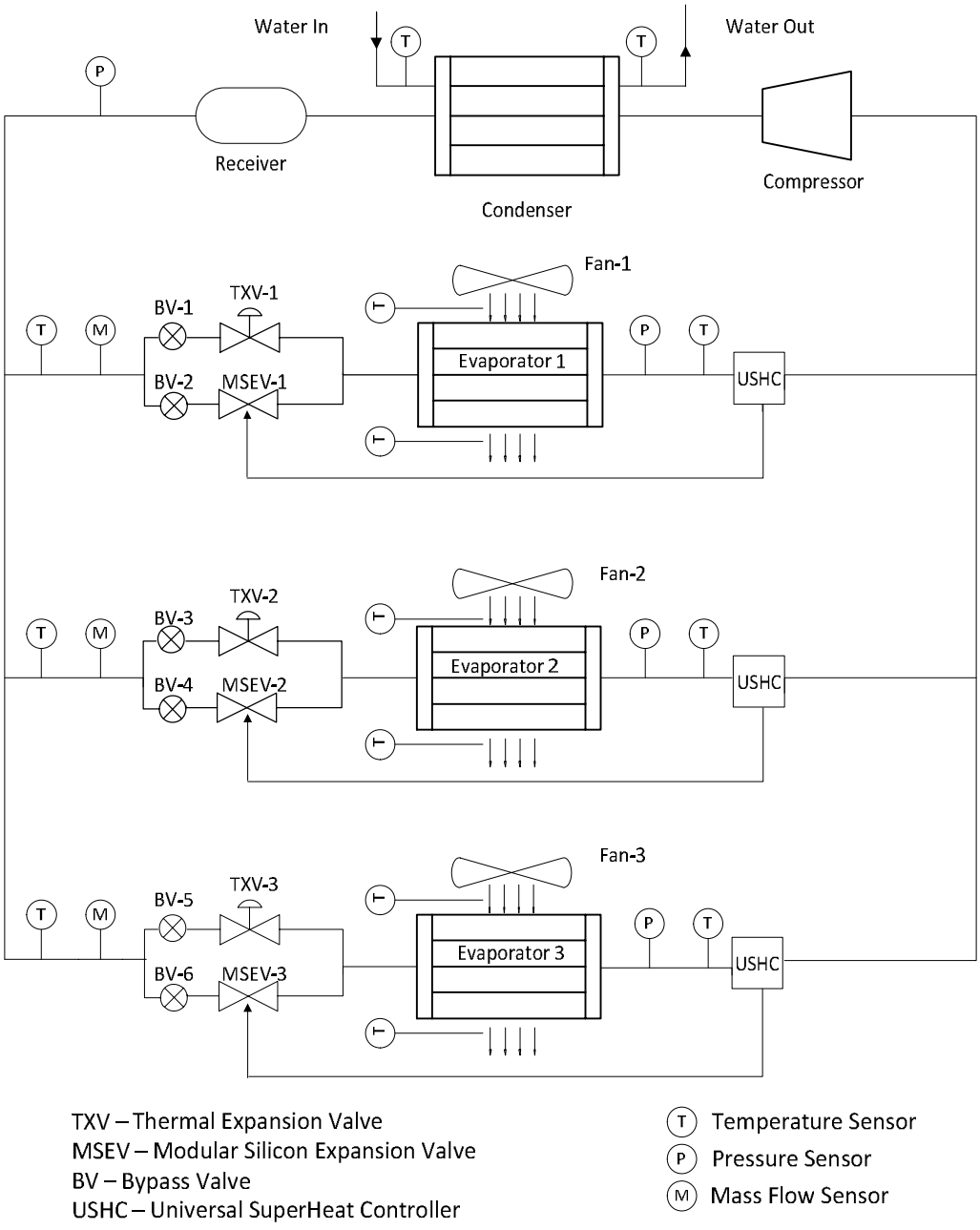

Figure 18: Schematic of Hussman System

2.2.1 Major Components

Compressor

The compressor installed on the Hussman system is manufactured by Ingersoll-Rand. It is a constant speed reciprocating type compressor with 1750 rpm. The supply voltage is 208/230V AC at 60 Hz. The following Figure 19 is a picture of the compressor.

Figure 19: Ingersoll-Rand Compressor

Condenser

The condenser of the system is a water cooled plate type heat exchanger manufactured by Swep International Inc. It has 80 parallel plated and the feature of single pass and counter current flow. Building chilled water is used as the supply water to the condenser. Building chilled water has inlet water at 6 ºC. The valve on the building chilled water line is set to fixed position. The chilled water is supplied at about 5 gpm. The condenser is shown in Figure 20.

Figure 20: Condenser

Evaporators

Three evaporators are installed on the Hussman system. All of them are finned tube heat exchangers. Total 120 plate type fins are on each evaporator. And each evaporator has two parallel aluminum tubes. Figure 21 shows one evaporator.

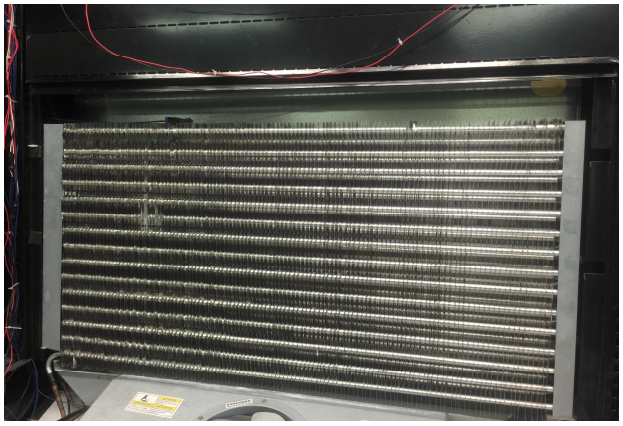

Figure 21: Evaporator

Evaporator Fans

There are three fans installed on the system as shown in Figure 22. The fans blow the air through the evaporator coils, where heat transfer happens between the coils and air. The fan speed can be controlled by the Smart Fan Speed Control Box.

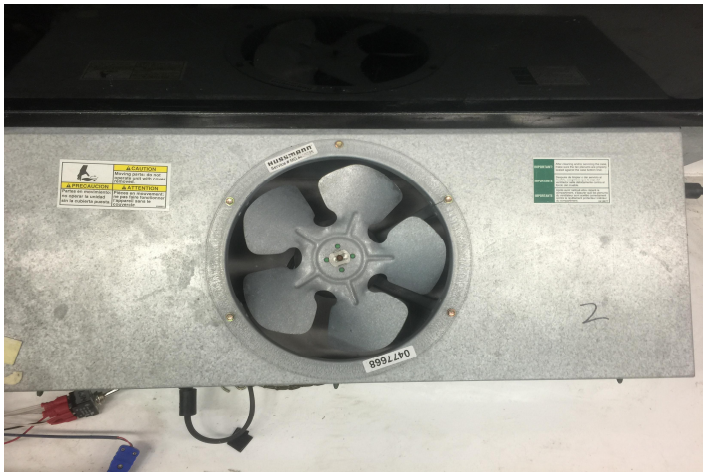

Figure 22: Evaporator Fan

Expansion Valves

Three thermal expansion valves (Figure 23) are installed parallel with the modular silicon expansion valve (Figure 24). Details of the modular silicon expansion valve were provided earlier in 1.2 in chapter 1.

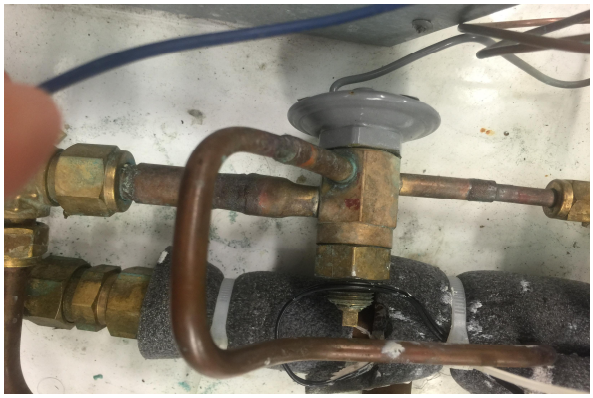

Figure 23: Thermal Expansion Valve

Figure 24: Modular Silicon Expansion Valve

2.2.2 Sensors

T-type thermocouples manufactured by Omega Inc. are used to measure the refrigerant temperature and air temperature in the system. Detailed description of this thermocouple is given in section 2.1.2. On the Hussman system, the thermocouples are connected to NI-cDAQ board 9213.

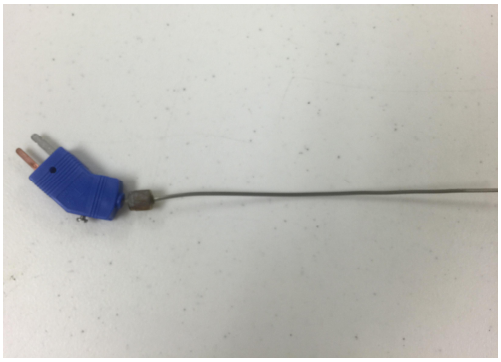

Figure 25: Thermocouple

Three mass flow meters are installed before the evaporators to measure the refrigerant flow. They are manufactured by McMillan Inc. Figure 26 shows the mass flow meter.

Figure 26: Mass Flow Meter

Four pressure transducers are used on the Hussman system. An example is shown in Figure 27. One is used to measure condenser pressure and three are used to measure the evaporator pressure.

Figure 27: Pressure Transducer

Three commercial superheat controllers called Universal Superheat Controller (USHC) manufactured by DunAn Microstaq are installed to control the MSEVs. Figure 28 gives an example of the USHC. There are also switches installed on the system so that the MSEV can be either controlled by USHC or the computer.

Figure 28: DMQ's Universal Superheat Controller

Data transmission between the USHC and the computer is finished by U-485G converter as shown in Figure 29.

Figure 29: USB-RS485 Converter

Figure 30 shows the NI-cDAQ 9172 and modules. It is connected through a USB port to the NI-cDAQ board in the computer.

Figure 30: NI-cDAQ 9172 and Modules

Table 2 lists the details of the components on the Hussman system.

Table 2: Components on the Hussman System

Part	Manufacturer	Part No.	Quantity
Compressor	Ingersoll Rand	IR2CO278SK	1
Condenser	Swep Inc.	B10THx80	1
Liquid Receiver	Refrigeration Specialties Group	3389	1
Thermal Expansion Valve	Sporlan	Unknown	3
Modular Silicon Expansion Valve	DunAn Microstaq	SH15K2	3
By-pass Valve	Swagelok	B-43S4	6
Universal Superheat Controller	DunAn Microstaq	SHC-G1.3	3
Evaporator Fans	Hussman	4410546	3
Fan Control Box	Control Resources	108V-800E	1
Thermocouple	Omega	GTMQSS-062U-6	11
Pressure Transducer	Omega	PX3.9-300G5V	4
Mass Flow Meter	McMillan	Model 102	3
Power Transducer	CR Magnetics	CR6210-250-50	1
USB-RS485 Converter	Donated by DMQ	Unknown	1

CHAPTER III

LEAKAGE RATE TEST

DunAn Mirostaq currently produces direct acting silicon expansion valves (PDA) as shown in Figure 31. Past research indicate that PDA valves are more capable of advanced control strategies, with repeatable operational behavior. The design of the PDAs gives them with small leakage rate and different cooling capacities. These characteristics give them a lot of potential applications like HVAC&R, electronics cooling, etc. In Chapter 3 and 4, the characteristics of eight direct acting silicon expansion valves (PDA) manufactured by DunAn Microstaq were experimentally examined. Chapter 3 describes the modification of the existing experimental equipment for the leakage rate test and the test results. In Chapter 4 details of the cooling capacity tests are presented.

Figure 31: PDA Manufactured by DMQ

3.1 Test Procedure

The experimental system used in this part the water chiller system as described in chapter 2 section 2.1. The device under test is the silicon expansion valve (PDA) manufactured by DunAn Microstaq (DMQ). The PDA is installed in the housing provided by DMQ which is powered by a 12 volts DC pulse-width-modulation control circuit. The housing is designed so that changing PDA module is easy. In total eight PDA models were tested. Figure 31 shows an example of a PDA. Figure 32 is a PDA installed in the housing provided.

Figure 32: PDA Installed in Housing

The inlet of the PDA to be tested was connected to the outlet of the condenser. A tank with a small amount of tow-phase R134a refrigerant was connected to the outlet of the PDA in the multi-evaporator water chiller refrigeration system. The modified schematic of the system is shown in Figure 33. The system pressure was measured using pressure gages connected to the data loggers and the pressure in the tank was determined by using the two phase assumptions of thermodynamics at a measured temperature. The system was run for 1 hour for each group of test, with one evaporator (evaporator #1) in normal operation and the other two closed. During the test time, the PDA connected at the outlet of condenser remained closed for the whole time. Before each test, 10 power cycles are applied to the PDA. 24 hours of resting time is given to the PDA before the test. The leak rate was found by measuring the mass added to the refrigerant tank during the test.

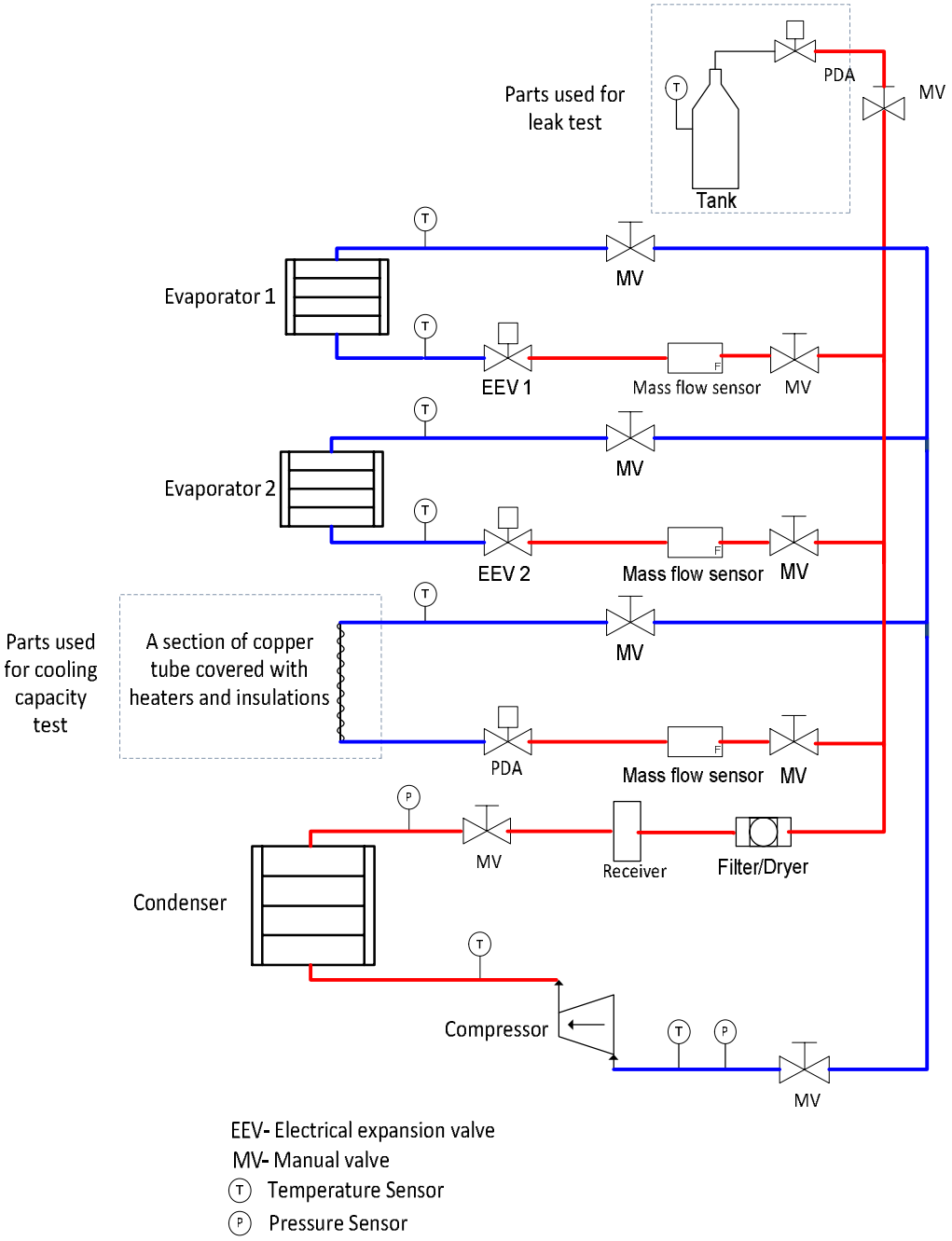

Figure 33: Modified Schematic of the Water Chiller System

In order to generate varied pressure differences across the PDA, the tank could be put into an iced water bucket or at room temperature, or the condenser water temperature could be changed. Due to the limited number of possible operating conditions, each valve has been tested under four pressure differences. While the system was running, an auxiliary heat exchanger connected to the building chilled water was used to maintain the condenser water temperature at a constant valve. At least 30 minutes of system running time is given before starting to collect the data. The uncertainty calculation procedure details are given in the appendices. Because the leak rate is very small, a mass scale with less than 1g uncertainty is critical to the accuracy of the leak tests. Sensitivity of major system components is given in the following Table 3.

Table 3: Sensitivity of Major System Components

Transducer	Sensitivity
Type T Thermocouples	0.5 °C
Pressure Transducer (Evaporator)	21 kPa
Pressure Transducer (Condenser)	21 kPa
Scale	0.5 g

3.2 Leak Rate Test Results

All of the leak rate results are plotted in Figure 34. Based on the leak rate, the valves are grouped into 3 groups. B2, X2 and C2 have the biggest leak rate. 3-10, 3-11 and 3-2 have the smallest leak rate. 4A and 5A are in the middle of the range. Magnified plots of these leak rate results are shown in Figure 35, Figure 36 and Figure 37. Detailed

leak rate data is included from Table 4 to Table 11. The trend lines shown are 2nd order polynomials fit using a least squares minimization criterion.

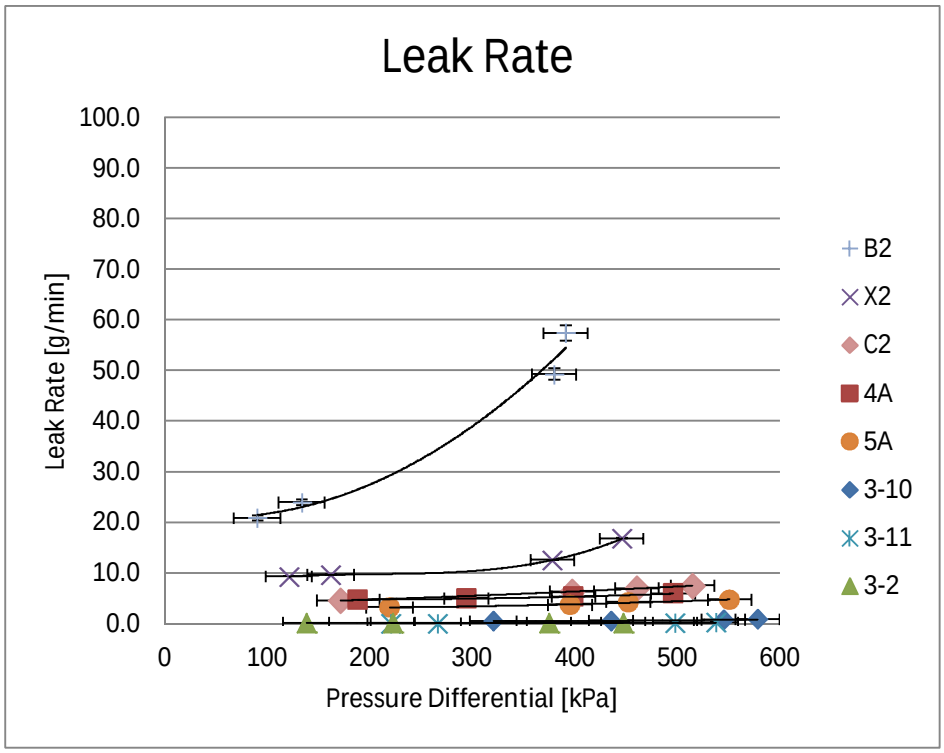

Figure 34: Leak Rate Plot

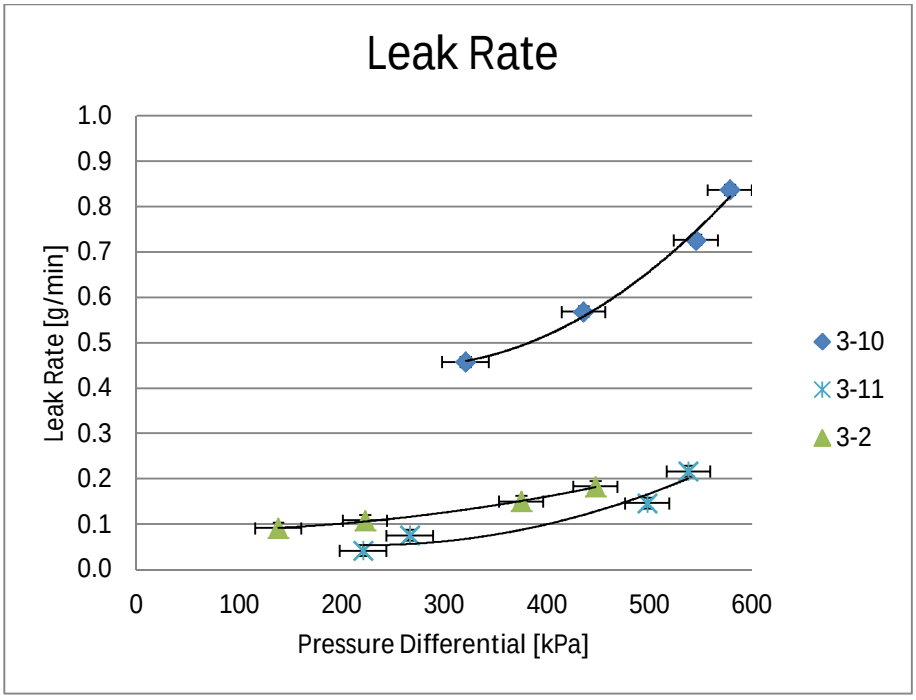

Figure 35: PDA 3-10, 3-11, 3-2 Leak Rate

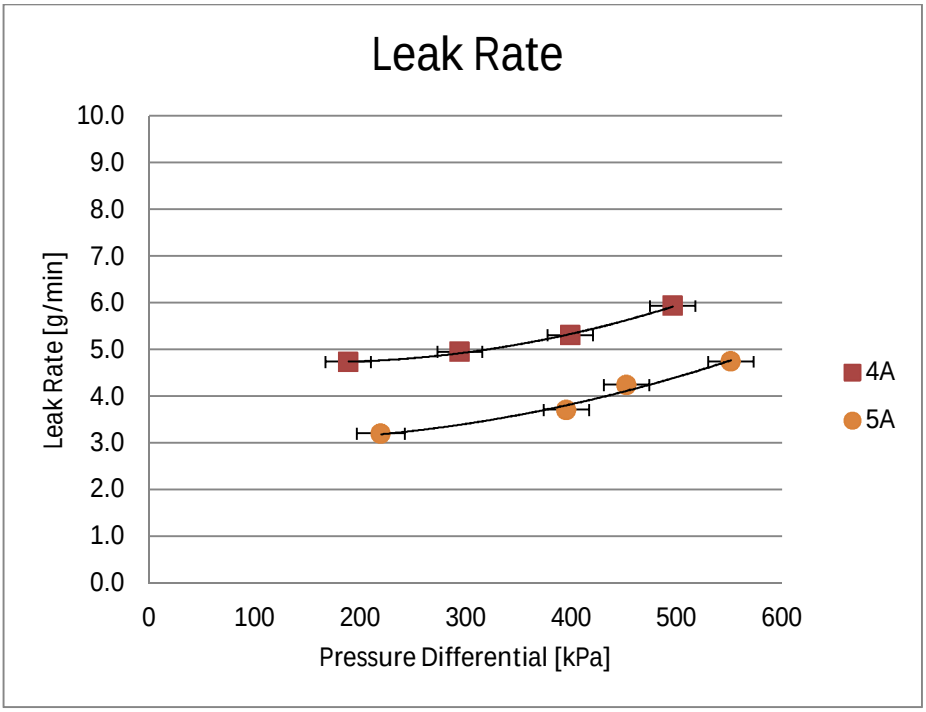

Figure 36: PDA 4A, 5A Leak Rate

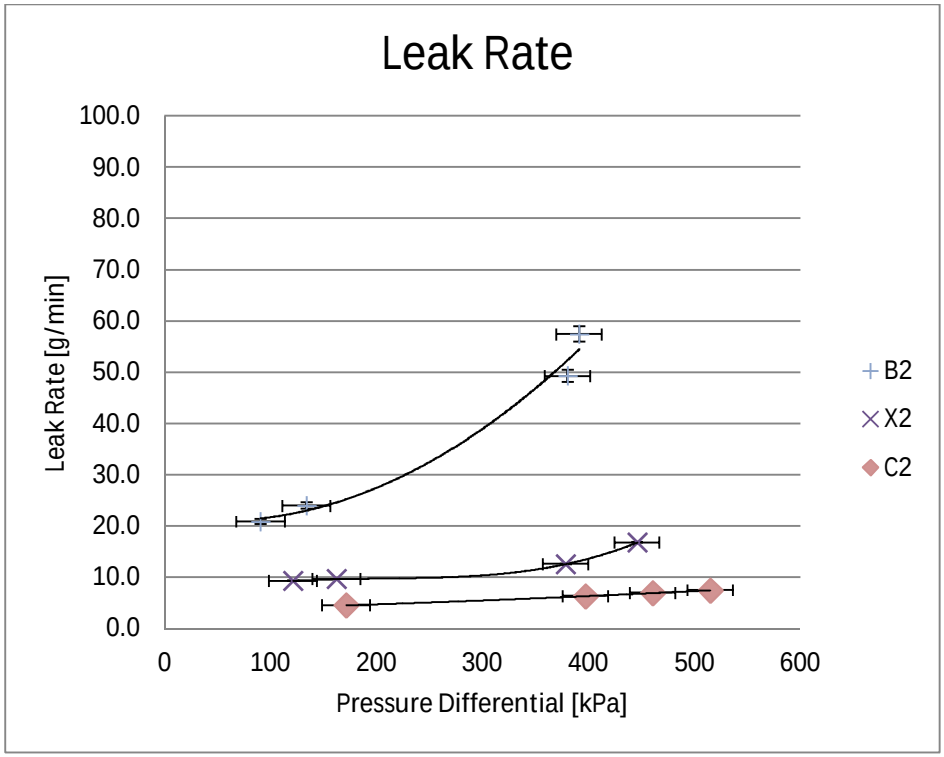

Figure 37: PDA B2, X2, C2 Leak Rate

Table 4: B2 Leak Test Data

Pressure (kPa)	Uncertainty (kPa)	Leak Rate (g/min)	Uncertainty (g/min)	Leak Rate (mg/sec)	Uncertainty (mg/sec)
91.0	22.7	20.843	0.503	347.39	8.39
134.2	22.7	23.948	0.609	399.14	10.15
380.4	21.4	49.268	1.146	821.14	19.10
391.6	21.5	57.409	1.489	956.82	24.81

Table 5: X2 Leak Test Data

Pressure (kPa)	Uncertainty (kPa)	Leak Rate (g/min)	Uncertainty (g/min)	Leak Rate (mg/sec)	Uncertainty (mg/sec)
121.7	22.7	9.300	0.040	0.66	155.00
162.6	22.8	9.635	0.041	0.68	160.59
378.7	21.4	12.587	0.046	0.77	209.78
446.1	21.4	16.782	0.061	1.02	279.71

Table 6: C2 Leak Test Data

Pressure (kPa)	Uncertainty (kPa)	Leak Rate (g/min)	Uncertainty (g/min)	Leak Rate (mg/sec)	Uncertainty (mg/sec)
171.6	22.8	4.548	0.020	75.80	0.19
461.0	21.4	6.936	0.023	115.60	0.19
397.6	21.4	6.336	0.022	105.60	0.19
515.3	21.4	7.488	0.024	124.80	0.19

Table 7: 4A Leak Test Data

Pressure (kPa)	Uncertainty (kPa)	Leak Rate (g/min)	Uncertainty (g/min)	Leak Rate (mg/sec)	Uncertainty (mg/sec)
189.0	21.4	4.733	0.014	78.89	0.23
294.7	21.4	4.950	0.014	82.50	0.24
399.3	21.4	5.308	0.015	88.47	0.24
496.4	21.4	5.933	0.015	98.89	0.25

Table 8: 5A Leak Test Data

Pressure (kPa)	Uncertainty (kPa)	Leak Rate (g/min)	Uncertainty (g/min)	Leak Rate (mg/sec)	Uncertainty (mg/sec)
220.0	22.7	3.200	0.013	53.33	0.21
395.8	21.4	3.706	0.013	61.76	0.22
452.6	21.5	4.242	0.013	70.69	0.23
551.5	21.5	4.742	0.013	79.03	0.23

Table 9: 3-10 Leak Test Data

Pressure (kPa)	Uncertainty (kPa)	Leak Rate (g/min)	Uncertainty (g/min)	Leak Rate (mg/sec)	Uncertainty (mg/sec)
320.9	22.8	0.458	0.011	12.63	0.19
436.0	21.4	0.568	0.011	13.82	0.19
545.4	21.4	0.726	0.011	16.05	0.19
578.6	21.4	0.837	0.011	18.68	0.19

Table 10: 3-11 Leak Test Data

Pressure (kPa)	Uncertainty (kPa)	Leak Rate (g/min)	Uncertainty (g/min)	Leak Rate (mg/sec)	Uncertainty (mg/sec)
221.3	22.8	0.042	0.012	0.69	0.20
266.6	22.8	0.075	0.012	0.13	0.20
498.3	21.5	0.147	0.012	2.44	0.19
538.3	21.5	0.217	0.012	3.61	0.20

Table 11: 3-2 Leak Test Data

Pressure (kPa)	Uncertainty (kPa)	Leak Rate (g/min)	Uncertainty (g/min)	Leak Rate (mg/sec)	Uncertainty (mg/sec)
138.5	22.6	0.092	0.012	7.63	0.20
223.1	21.5	0.108	0.012	9.47	0.20
375.3	21.4	0.150	0.012	12.11	0.20
447.5	21.4	0.183	0.012	13.95	0.20

Based on the test results, B2 has the highest leak rate. And 3-2 has the smallest leak rate. The leak rate results have the following relationship:

$$B2 > X2 > 4A > 5A > 3-10 > 3-11 > 3-2$$

The calculated uncertainty includes both random and bias uncertainties. The uncertainty of leak rate of all the tests is less than 5%. Due to the relatively big leak rate of B2 and X2 valves, in order to maintain a constant system pressure, the test running duration of X2 is reduced to 28 minutes. And B2 has 4 minutes of system running time. But they still have an uncertainty under 5%. The details of uncertainty calculation are given in Appendices.

CHAPTER IV

COOLING CAPACITY TEST

Cooling capacity of an expansion valve refers to the heat absorbed by the refrigerant. It can be calculated by the difference of the enthalpy from the inlet of the evaporator to the outlet of the evaporator multiplied by the refrigerant mass flow rate. The associated equation is given blow:

$$Q = \dot{m}(h_{outlet} - h_{inlet}) \quad (1)$$

where h_{inlet} is the inlet enthalpy to the evaporator, and h_{outlet} is the outlet enthalpy to the evaporator. $\dot{m}$ is the refrigerant mass flow rate, which is a function of pressure differential and the valve opening position during the experimental tests. At the evaporator outlet, the refrigerant is maitained a 5 °C superheated vapor. Knowing the pressure and temperature of the evaporator outlet, h_{outlet} can be obtained from thermodynamic properties. Valve throttling is assumed to be an isenthalpic process in which the enthalpy of the refrigerant remains constant. So the enthalpy before the valve equals the enthalpy after the valve. Thus h_{inlet} can be determined from thermodynamic properties using condenser pressure, P_c and condenser refrigerant outlet temperature, T_{cro}.

4.1 Test Procedure

The PDA valve was installed on the multi-evaporator water chiller refrigeration system in parallel with current electrical expansion valves. Evaporator 3 has been

replaced by a section of copper tube (shown in Figure 38). To provide a heating load for the refrigeration system, electrical strip heaters were placed on a simple copper heat exchanger. Four heaters with 50W capacity were used with an electronic control system that could affect a small step increase in head load. An example is shown in Figure 39. The electrical power was provided to the heaters, and electrical (heating) power was measured. The electrical connections are shown in Figure 40. A Proportional-Integral controller was used to change valve position to regulate evaporator superheat to 5°C, while the strip heaters were given step increases (or decreases) of heat. The heating power should be equal to the cooling capacity in ideal condition. For the PDAs, the mass flow rates are relatively small and below the sensing range of the mass flow meters. Thus the cooling capacity was obtained by measuring the heating power.

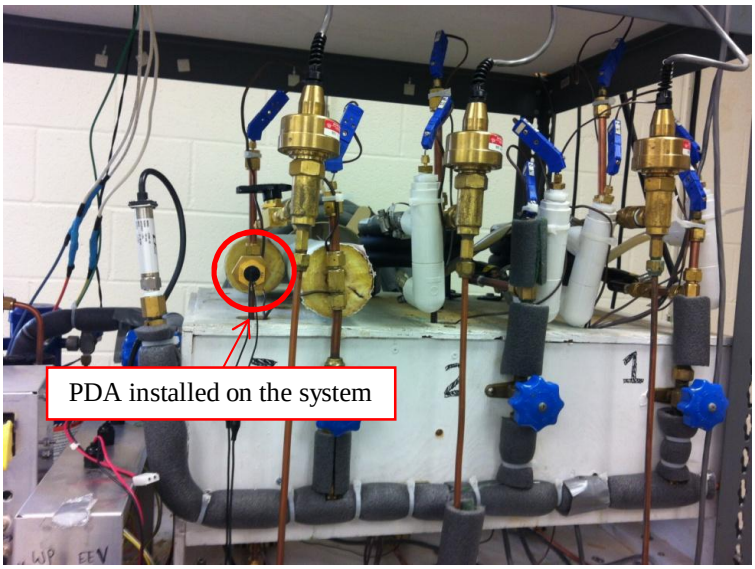

Figure 38: PDA Installed Parallel with the EEV on Water Chiller System

Figure 39: Strip Heater

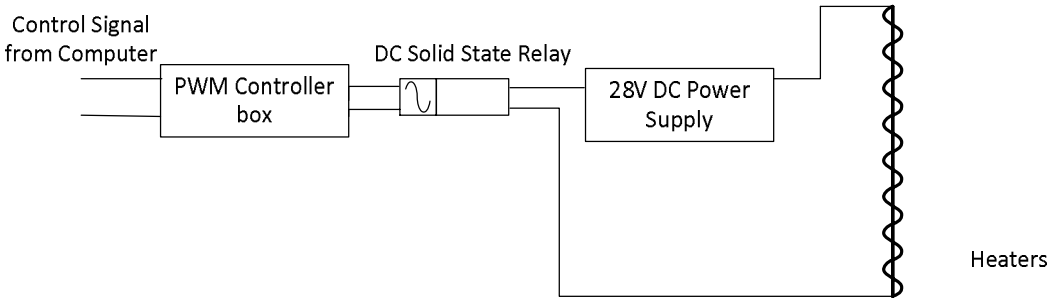

Figure 40: Strip Heater Connection

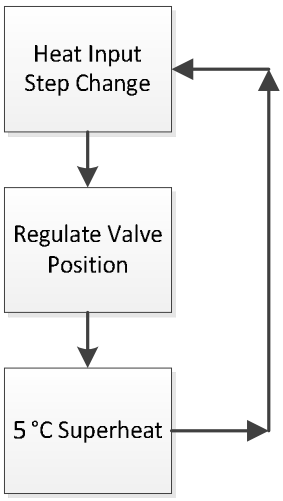

Figure 41: Cooling Capacity Test Procedure

Each valve has been tested under three pressure differences. One group of capacity test would take several hours to finish. Operating the system for long time would lead to a slow increase in condenser water temperature, which would cause system pressure change. So an extra heat exchanger connected to the building chilled water was used to maintain a constant condenser water temperature. Small step increases were given to the strip heaters. During each step, at least 2500 data points have been collected for data analysis so that the system random error was negligible compared to the system sensor error.

4.2 Cooling Capacity Results

4.2.1 PDA X2

For the PDA X2, the maximum cooling capacity was beyond the limits of the existing equipment. The tests only covered from 0% valve open position to 71% valve open position as shown in Figure 42. Following the trend of the line, the maximum cooling capacity of X2 is estimated to be 380W. Detailed data points are given in Table 12.

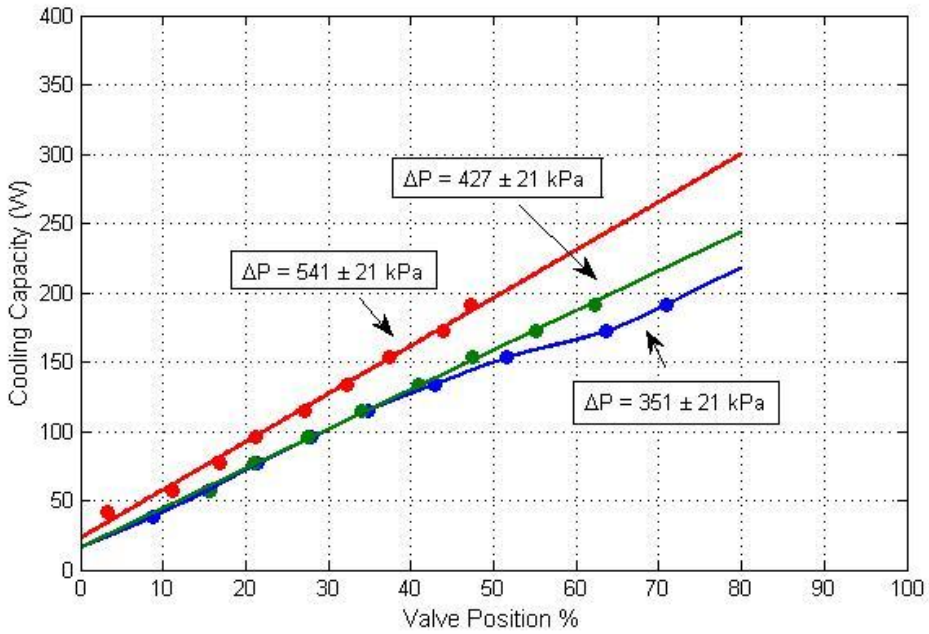

Figure 42: PDA X2 Cooling Capacity Results

Table 12: PDA X2 Cooling Capacity Data

ΔP = 541 ± 21 kPa			ΔP = 427 ± 21 kPa			ΔP = 351 ± 21 kPa		
Heat (W)	Valve %	Superheat (°C)	Heat (W)	Valve %	Superheat (°C)	Heat (W)	Valve %	Superheat (°C)
42.1	3	4.9±0.7	57.5	16	5.1±0.7	38.3	9	5.4±0.7
57.5	11	5.0±0.7	76.6	21	5.0±0.7	57.5	15	5.5±0.7
76.6	17	5.0±0.7	95.8	27	5.1±0.7	76.6	21	5.2±0.7
95.8	21	5.0±0.7	114.9	34	5.3±0.7	95.8	28	5.1±0.7
114.9	27	5.0±0.7	134.1	41	5.0±0.7	114.9	35	5.0±0.7
134.1	32	5.0±0.7	153.2	47	5.1±0.7	134.1	43	5.0±0.7
153.2	37	5.0±0.7	172.4	55	5.0±0.7	153.2	52	5.0±0.7
172.4	44	5.0±0.7	191.5	62	5.0±0.7	172.4	64	5.0±0.7
191.5	47	5.0±0.7				191.5	71	5.0±0.7

4.2.2 PDA 5A

From Figure 43, PDA 5A has a maximum cooling capacity of 77W. From 30% to 90% valve position, the relationship between valve position and cooling capacity is basically linear. The cooling capacity reaches a maximum between 90% and 100% valve opening. Detailed experimental data is shown in Table 13.

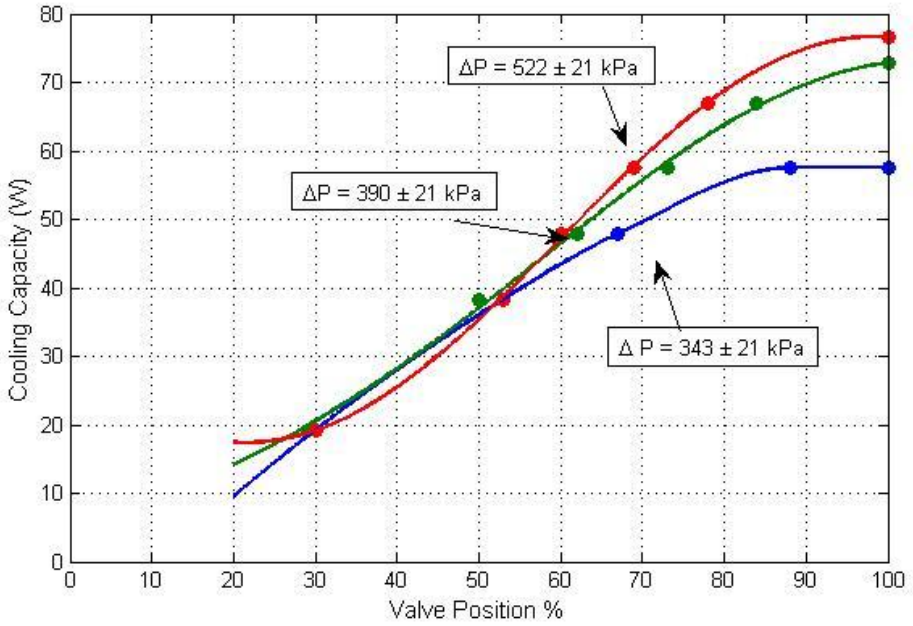

Figure 43: PDA 5A Cooling Capacity Results

Table 13: PDA 5A Cooling Capacity Data

ΔP = 343 ± 21 kPa			ΔP = 390 ± 21 kPa			ΔP = 522 ± 21 kPa		
Heat (W)	Valve %	Superheat (°C)	Heat (W)	Valve %	Superheat (°C)	Heat (W)	Valve %	Superheat (°C)
19.2	30	6.0±0.7	19.2	29	5.6±0.7	19.2	30	2.9±0.7
38.3	53	5.1±0.7	38.3	50	5.3±0.7	38.3	53	5.7±0.7
47.9	67	5.0±0.7	47.9	62	5.2±0.7	47.9	60	4.7±0.7
57.5	88	5.0±0.7	57.5	73	5.0±0.7	57.5	69	5.0±0.7
57.5	100	4.9±0.7	67.0	84	5.1±0.7	67.0	78	5.0±0.7
			72.8	100	5.1±0.7	76.6	100	4.7±0.7

4.2.3 PDA 3-10

PDA 3-10 has a maximum capacity of 161W. At approximately 30% valve opening, PDA 3-10 has 20W cooling capacity. Detailed experimental data is shown in Table 14.

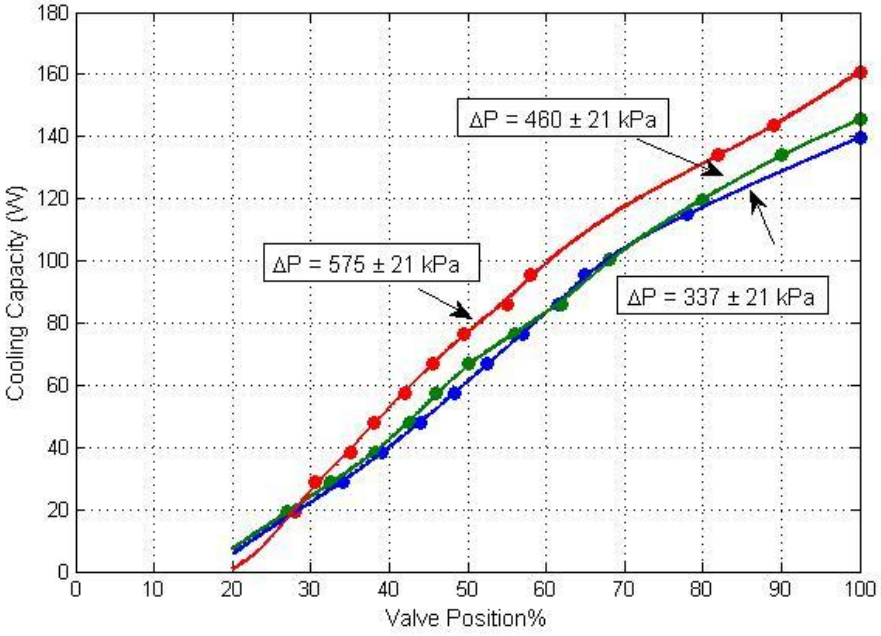

Figure 44: PDA 3-10 Cooling Capacity Results

Table 14: PDA 3-10 Cooling Capacity Data

ΔP = 338 ± 21 kPa			ΔP = 460 ± 21 kPa			ΔP = 575 ± 21 kPa		
Heat (W)	Valve %	Superheat (°C)	Heat (W)	Valve %	Superheat (°C)	Heat (W)	Valve %	Superheat (°C)
19.2	28	2.3±0.7	19.2	27	6.3±0.7	19.2	28	4.6±0.7
28.7	35	2.9±0.7	28.7	33	5.7±0.7	28.7	30	4.7±0.7
38.3	39	5.6±0.7	38.3	38	5.0±0.7	38.3	35	5.0±0.7
47.9	44	5.2±0.7	47.9	43	5.0±0.7	47.9	38	4.3±0.7
57.5	48	5.8±0.7	57.5	46	3.6±0.7	57.5	42	5.0±0.7
67.0	53	4.9±0.7	67.0	50	4.8±0.7	67.0	46	5.0±0.7
76.6	57	4.9±0.7	76.6	56	5.2±0.7	76.6	50	5.3±0.7
86.2	62	4.5±0.7	86.2	62	5.8±0.7	86.2	55	5.3±0.7
95.8	65	4.9±0.7	100.5	68	4.8±0.7	95.8	58	4.8±0.7
114.8	78	5.0±0.7	119.6	80	5.0±0.7	134	82	5.1±0.7
139.7	100	5.2±0.7	134.0	90	5.1±0.7	143.6	89	5.3±0.7
			145.5	100	4.9±0.7	160.8	100	5.2±0.7

4.2.4 PDA 3-11

PDA 3-11 has a maximum capacity of 157 W. The trend lines show PDA 3-11 has a linear relationship between cooling capacity and valve opening position. Detailed experimental data is shown in Table 15.

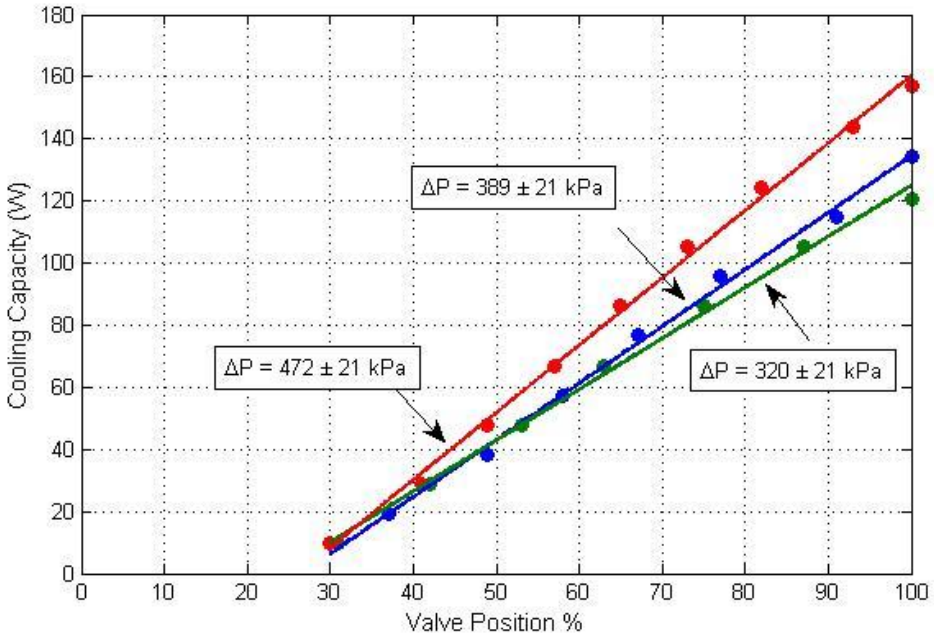

Figure 45: PDA 3-11 Cooling Capacity Results

Table 15: PDA 3-11 Cooling Capacity Data

ΔP = 320 ± 21 kPa			ΔP = 389 ± 21 kPa			ΔP = 472 ± 21 kPa		
Heat (W)	Valve %	Superheat (°C)	Heat (W)	Valve %	Superheat (°C)	Heat (W)	Valve %	Superheat (°C)
9.6	31	4.8±0.7	19.2	37	6.0±0.7	9.6	30	5.3±0.7
28.7	42	4.8±0.7	38.3	47	4.8±0.7	28.7	41	5.7±0.7
47.9	53	1.9±0.7	57.5	58	5.1±0.7	47.9	49	5.5±0.7
67.0	63	5.0±0.7	76.6	67	5.1±0.7	67.0	57	4.8±0.7
86.2	75	5.0±0.7	95.8	77	4.8±0.7	86.2	65	4.9±0.7
105.3	87	5.5±0.7	114.9	91	4.9±0.7	105.3	73	5.6±0.7
120.7	100	4.6±0.7	134.1	100	5.2±0.7	124.5	82	4.8±0.7
						143.6	93	5.4±0.7
						157.0	100	5.3±0.7

PDA 3-10, PDA 3-11 and 5A were tested for the full valve operation range. X2 was tested from 0% to 71% valve operation range due to system limitations. In order to validate the trend line of PDA X2, the heat exchanger with strip heaters and insulation has been replaced by a water-to-refrigerant heat exchanger. X2 was opened to 100% and the evaporator water flow rate was carefully adjusted to maintain a constant 5 °C superheat. The test failed to give a reasonable result as the X2 did not respond to the control signal to the test.

CHAPTER V

QUANTIFYING EFFICIENCY GAINS OF REFRIGERATION SYSTEMS USING ADVANCED SEV CONTROL ALGORITHMS

The characteristics of silicon expansion valves make them a good choice as an advanced throttling device in the refrigeration systems. In this chapter, DMQ's modular silicon expansion valves (MSEV) will be installed on a multi-evaporator Hussman commercial refrigeration system. A comprehensive set of experimental tests that will identify the most effective elements of an advanced valve control strategy under a variety of operating conditions.

The experimental system used in this part of research in the Hussman commercial refrigeration unit. Detailed information about the system is given in Chapter 2, section 2.2.

Several important values are calculated in this section to compare the performance between different control mechanisms.

$$Q_{refrigerant} = \dot{m}(h_{outlet} - h_{inlet}) \quad (2)$$

Equation (2) calculated the cooling from the refrigerant side, where h_{inlet} is the inlet enthalpy to the evaporator, and h_{outlet} is the outlet enthalpy to the evaporator. Mass flow rate is a function of pressure differential and the valve opening position during the experimental tests. At the evaporator outlet, the refrigerant is superheated vapor.

Knowing the pressure and temperature of the evaporator outlet, h_{outlet} can be obtained from thermodynamic properties. Valve throttling is assumed to be an isenthalpic process in which the enthalpy of the refrigerant remains constant. So the enthalpy before the valve equals the enthalpy after the valve. Thus h_{inlet} can be determined from thermodynamic properties using condenser pressure, P_c and condenser refrigerant outlet temperature, T_{cro}.

$$Q_{air} = c_p \dot{m}_{air} \left(T_{air\_out} - T_{air\_in} \right) \tag{3}$$

Equation (3) calculated the cooling from the air side. c_p is the heat capacity of air. $\dot{m}_{air}$ is the air flow rate going through the evaporator fans, which is obtained from Figure 46. T_{air_out} and T_{air_in} are temperature measurements from the thermocouples installed at fan inlet and evaporator outlet.

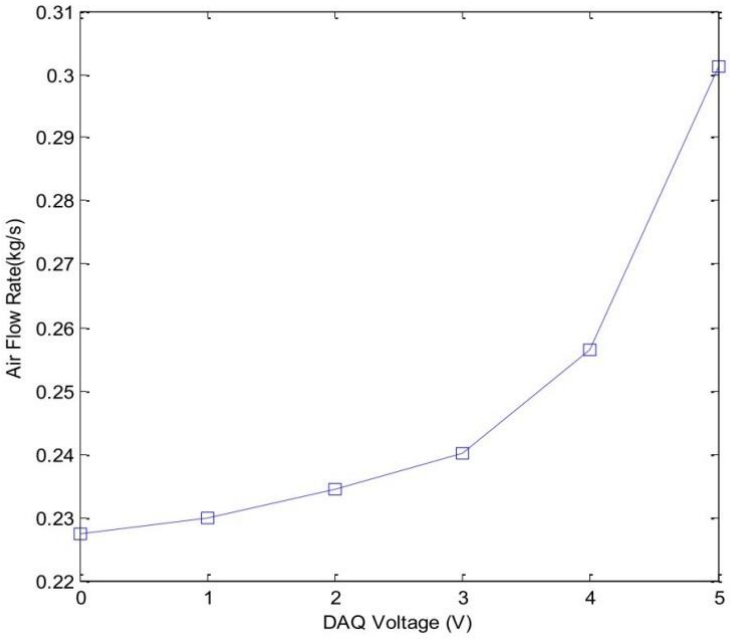

Figure 46: DAQ Voltage vs. Air Flow Rate [21]

Average cooling per cycle is defined by equation (4). One cycle is defined as the period of time that the compressor needs to turn on and turn off once. In equation (4), T is the cycle time. t is integrating time. $Q_{Cooling}(t)$ is the cooling gained by the system as a function of time. The Coefficient of Performance or the COP of the system is defined by equation (5). Q represents the cooling gained by the system and W is work input to the system.

$$Q_{ave} = \frac{\sum_{t}^{t+T} Q_{Cooling}(t)}{T} \tag{4}$$

This equation gives the cooling ability of the system for each on-off cycle.

$$COP = \frac{\sum Q}{\sum W} \tag{5}$$

Usually in supermarkets, the refrigeration systems run for 24 hours a day with periodic compressor on-off cycles with two or more defrost cycles each day. The compressor on-off cycle is automatically triggered by the discharge air temperature thermostat installed in these supermarket refrigeration display cases. In our experimental system, the unit is designed to shut off when the discharge air temperature falls to -1.1˚C (30 ˚F).

For all tests, the superheat set point is set to 8°C. Tests are conducted under several different conditions. Across these conditions, several main factors will be evaluated: efficiency improvement from TXV to MSEV, efficiency change by using different control strategies and refrigerant pull-down. Pull-down refers to the process of bringing the evaporator pressure down to the desired level at compressor start-up. This traps the refrigerant on each side of the compressor which preserves a pressure differential.

All the tests have been classified into two cases. The cases will each be run for the 5 configurations shown in Table 16.

Case 1: Run the system for two hours to get several repeatable fixed time compressor on-off cycles.

Case 2: Run the system for two hours to get several fixed thermostat set point on-off cycles. Discharge air temperature: -1.1 ˚C (30 ˚F)

Table 16: Five Configurations for Testing

1	TXV
2	MSEV + USHC
3	MSEV + custom algorithm (cascaded controller)
4	MSEV + USHC + valve shut off
5	MSEV + algorithm (cascaded controller)+ valve shut off

Configuration 1 will be a base line for the other tests. The comparison of configuration 1 and 2 will show the efficiency differences of thermal expansion valves vs. DMQ MSEVs. Configuration 2 and 3 are designed to compare a cascaded control algorithm with DMQ's commercial superheat controller (USHC). A specific refrigerant change control strategy: expansion valve shut off will be investigated in configuration 4 and 5. Both the cascaded controller and USHC were further tested in the low temperature condition and medium temperature to examine the performance, across a range of operating conditions.

5.1 Cascaded Controller Development

A cascaded controller has two feedback control loops. The first control loop determines the evaporator pressure setpoint. The second control loop determines the valve opening. One of the advantages of using a cascaded control loop is that it compensates for the nonlinearity of the system [6]. Another benefit of using a cascaded algorithm is that it can be effectively used to control multi-evaporator systems [6]. The cascaded control architecture can provide superior superheat regulation results for the multi-evaporator system based on the Silicon Expansion Valves in Ankush Gupta's research [21]. The same control methodology was implemented to regulate the superheat

for individual evaporators of the supermarket refrigeration system. The MSEVs accept a 0% to 100% valve opening signal from the DAQ PC which is converted to a 0-5 V pulse width modulation (PWM) voltage signal which in turn controls the valve opening. The schematic structure of the cascaded controller is shown in Figure 47.

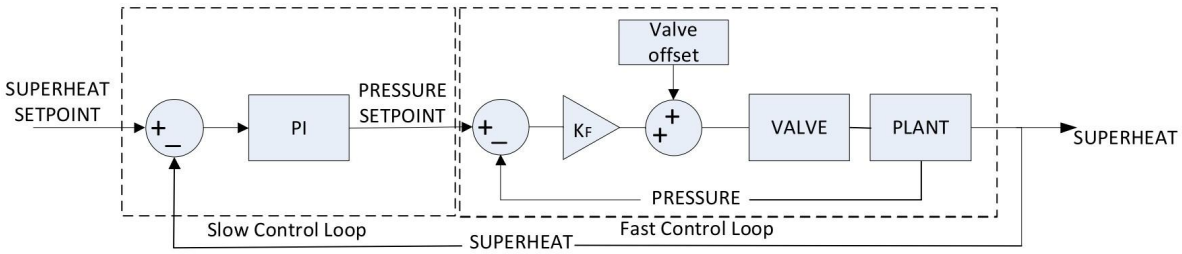

Figure 47: Schematic Structure of Cascaded Controller

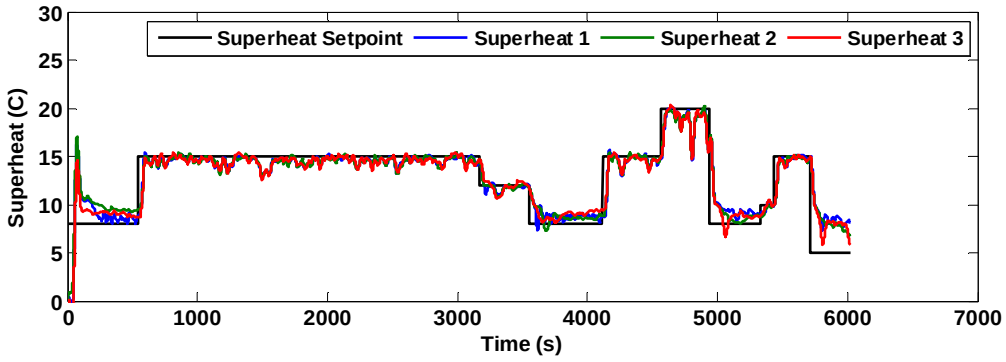

Figure 48: Superheat Change Test

In Figure 48, the MSEVs reached the superheat set point in 220 seconds after start up. When the superheat set point changed, the MSEVs responded immediately to

quickly track the superheat setpoint. This demonstrates the cascaded controller's quick response time and ability to reach operating conditions.

5.2 Fixed Thermostat Set Point On-off Cycles

In this test case, for each test configuration, the system was running for at least two hours to get several fixed thermostat set point on-off cycles. The discharge air temperature is -1.1 ˚C (30 ˚F). In the entire test, the superheat set point is set to 8°C.

5.2.1 TXV

Figure 49 shows 5 cycles of mass flow rate, superheat and refrigerant side cooling when the system was running with TXVs. From the results, we can see the TXVs cannot stabilize superheat well. We are losing superheat in evaporator 3 in each cycle. We can notice that superheat is not zero during compressor shut down; this is due to the fact that the evaporator fans were still on after the compressor shutdown which leads to the boiling of the refrigerant.

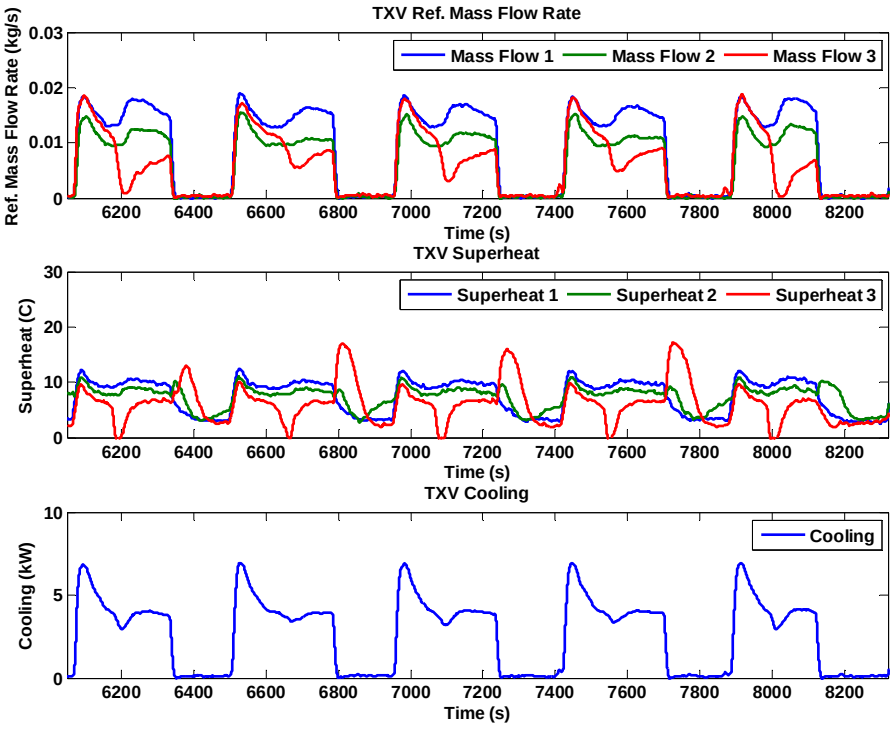

Figure 49: System Parameters with TXVs - Case 1

5.2.2 MSEV + USHC

Figure 50 shows the system parameters when the system was running with MSEVs and USHC. System superheat setpoint is 8 °C. DMQ's USHC can regulate superheat better than the TXV. But from the superheat plot, during each cycle, the controller didn't bring the superheat down to 8 °C. In the refrigerant mass flow rate plot, there was some mass flow during the off cycles. Due to non-zero mass flow rate and running fans during the off cycles, certain amount of cooling was gained during the off cycles.

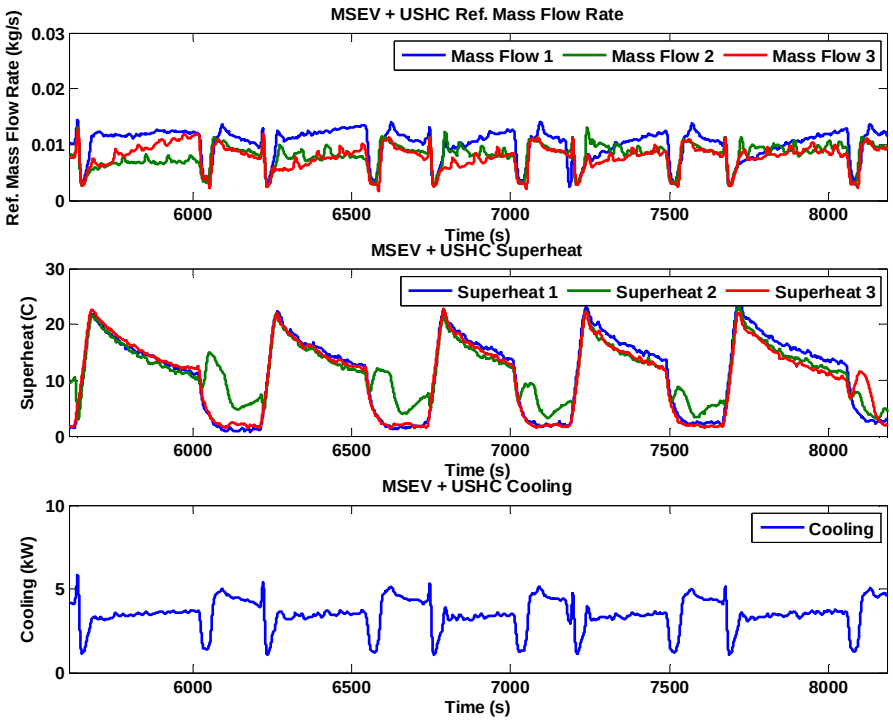

Figure 50: System Parameters with MSEVs and USHC - Case 1

5.2.3 MSEV + Cascaded Controller

In Figure 51, Superheat set point is 8°C. From the superheat plot, the cascaded controller can stabilized superheat 2 and 3 to 8°C and superheat 1 to 10°C. The controller was left running during the compressor down time. The MSEVs were not completely closed during the down time.

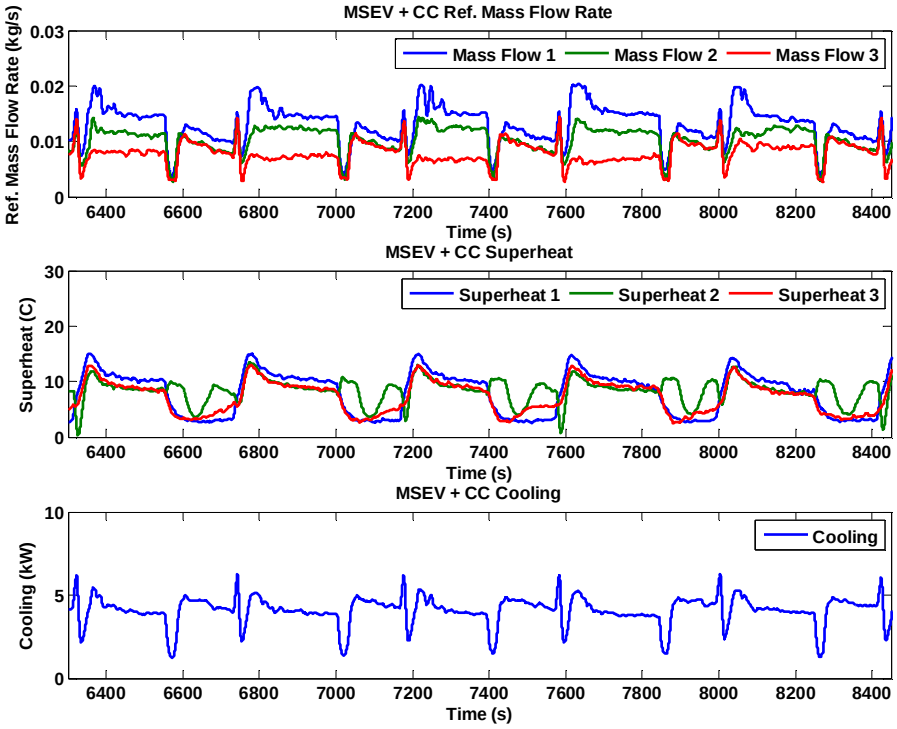

Figure 51: System Parameters with MSEVs and Cascaded Controller - Case 1

Figure 52 shows the comparison between the following three actuating mechanisms. MSEVs with cascaded controller have average cooling per cycle over 40W. MSEVs with USHC have average cooling per cycle around 35W. Then TXV has less than 30W average cooling per cycle.

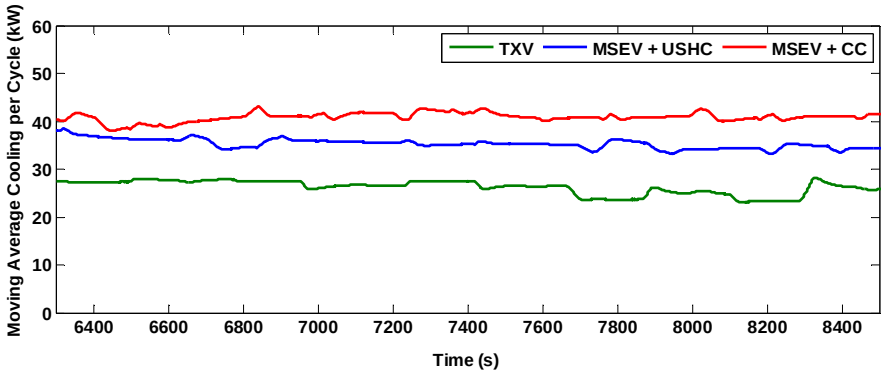

Figure 52: Moving Average Cooling per Cycle - Case 1

Table 17: Comparison of Performance Indicators for Five Compressor On-Off Cycles

	TXV	MSEV + USHC	MSEV+CC
Cooling (kW)	26	35	41
Power (kW)	16	15	16
COP	1.7	2.3	2.6
COP improvement compared to TXV	-	35%	53%

The data points listed in the table above are the average for five compressor on-off cycles. By analyzing this data, we find significant gain in the COP of the system with the use of the cascaded controller (+53 %) and the USHC (+35%) as compared to the TXVs. The cascaded controller showed the ability to regulate the superheat better compared to the other two configurations.

5.2.4 Cascaded Controller + Valve shut off

The valve shut off signal was given to the MSEVs when the compressor automatically shut off. Refrigerant mass flow rate, superheats and cooling for five cycles were given in Figure 53. In Figure 53, the valve off cycles were highlighted in the black dash line. The mass flow rate did not reach zero during the off cycles which indicated the MSEVs didn't fully close during the off cycles. In Figure 54, the PWM signals were plotted. In the dash circles, the PWM signals were 0% during the off cycles.

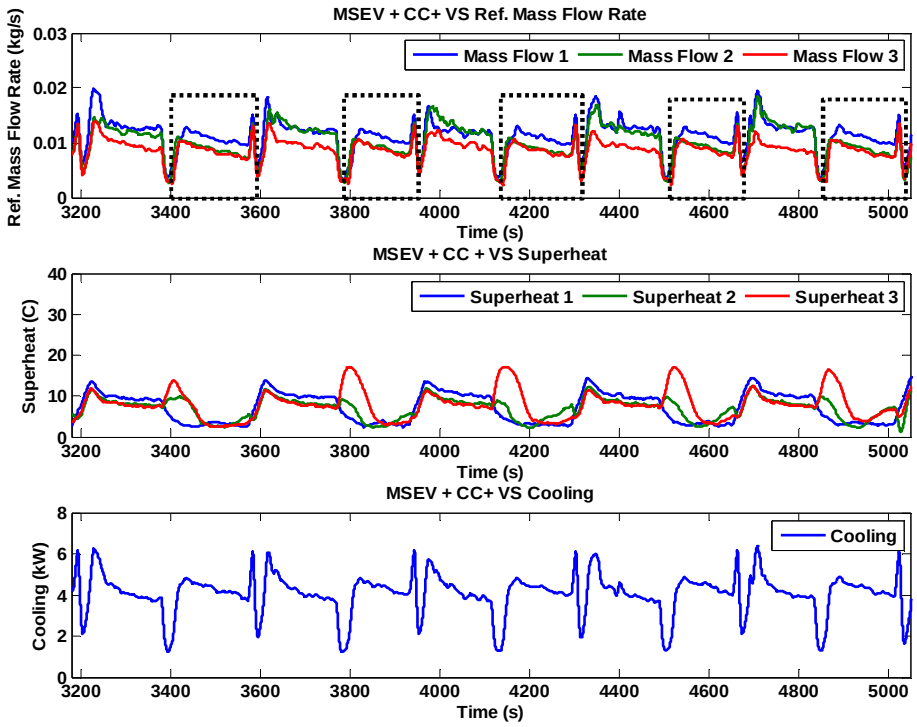

Figure 53: MSEVs with Cascaded Controller and Valve Shut off - Case 1

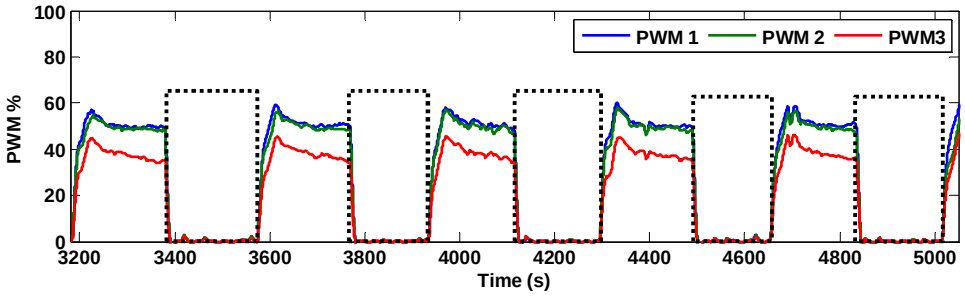

Figure 54: PWM Signals Sent to the MSEVs - Case 1

Another test was done to determine if the MSEVs were receiving the right signals, and if the ball valves before TXVs were leaking. The refrigerant mass flow rate was plotted in Figure 55. With the system running, MSEV 1 was given a 0 control signal. Mass flow 1 immediately went down. But instead of reaching 0, MSEV 1 still has 0.005kg/s mass flow rate. After 100s, the controller was turned back on, 70% PWM signal was given back to MSEV 1. Mass flow 1 went up to 0.02kg/s. In step 2, the ball valve before MSEV 2 was manually shut off. At the same time, mass flow 1 went down to 0 kg/s. The same procedures were repeated on MSEV 2 and MSEV 3. Mass flow 2 and mass flow 3 responded the same as mass flow 1. In step 7, the valve shut off signals were given by the computer. Mass flow 1, 2 and 3 went down and then went up again, but when the pressure differential went to 0 kPa, the mass flow went down to zero again.

From this test, one conclusion can be made. The ball valves before MSEVs function normally without any issues. The control signals fed to MSEVs are correct. The MSEVs respond to the control signals correctly. The mass flow during the off cycles is due to the structure of the MSEVs. MSEV is a spool valve. When the compressor was

turned off, there was still a certain amount of pressure difference on the MSEV. Due to pressure difference, the spool inside the MSEV was pushed to move which gives the refrigerant space to pass through the MSEV. When the pressure difference went to zero, mass flow went to zero at the same time.

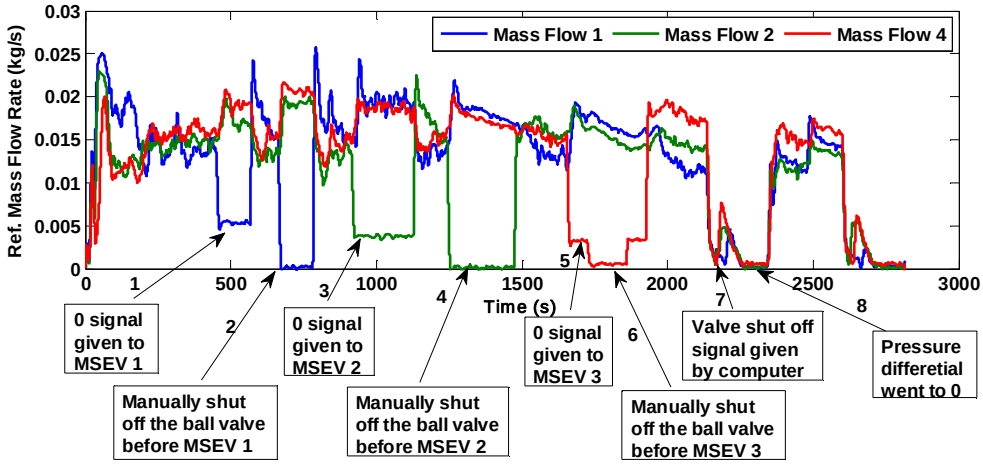

Figure 55: MSEVs Shut off Test

5.2.5 MSEV+ Manually Valve Shut off

A group of tests with manual shut off of the ball valves before the MSEVs during the off cycles were done. The system parameters were shown in Figure 56. Under the same environmental condition and test condition, the system was running again with the cascaded controller in Figure 59 as a comparison group.

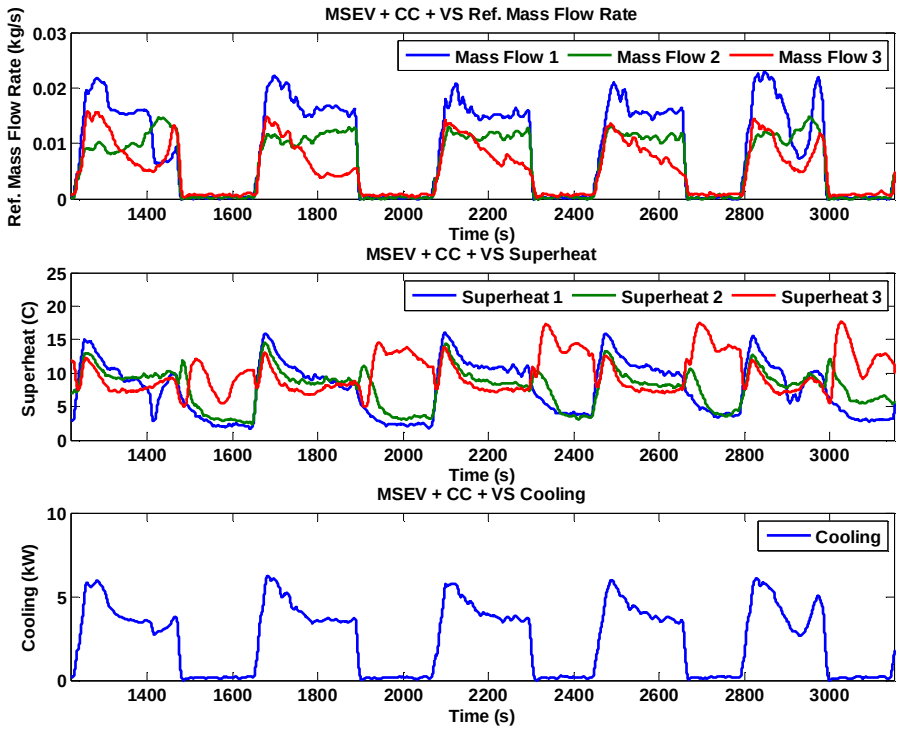

Figure 56: MSEVs with Cascaded Controller and Manual Valve Shut off - Case 1

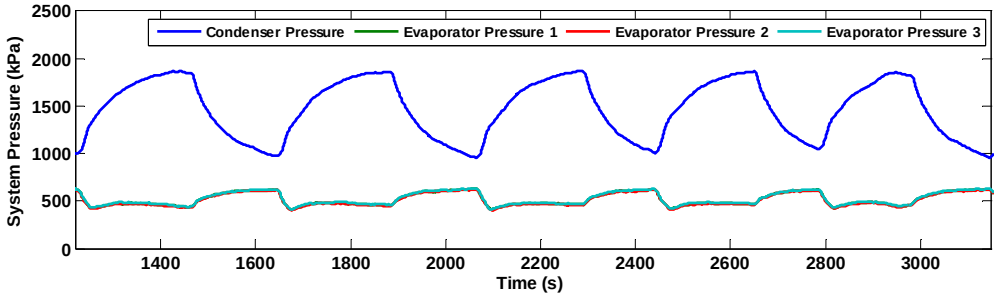

Figure 57: System Pressure - Case 1

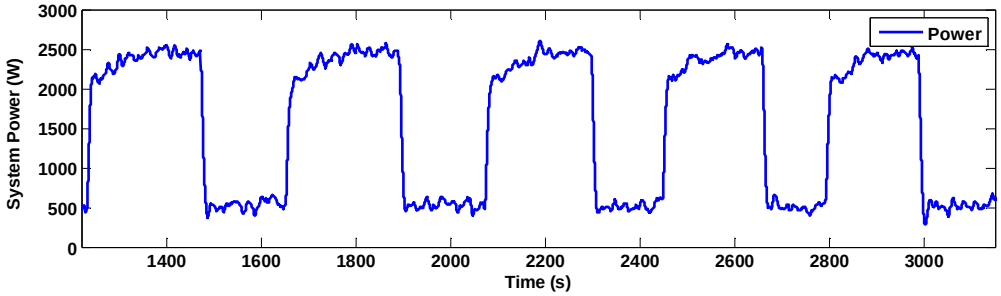

Figure 58: System Power Consumption - Case 1

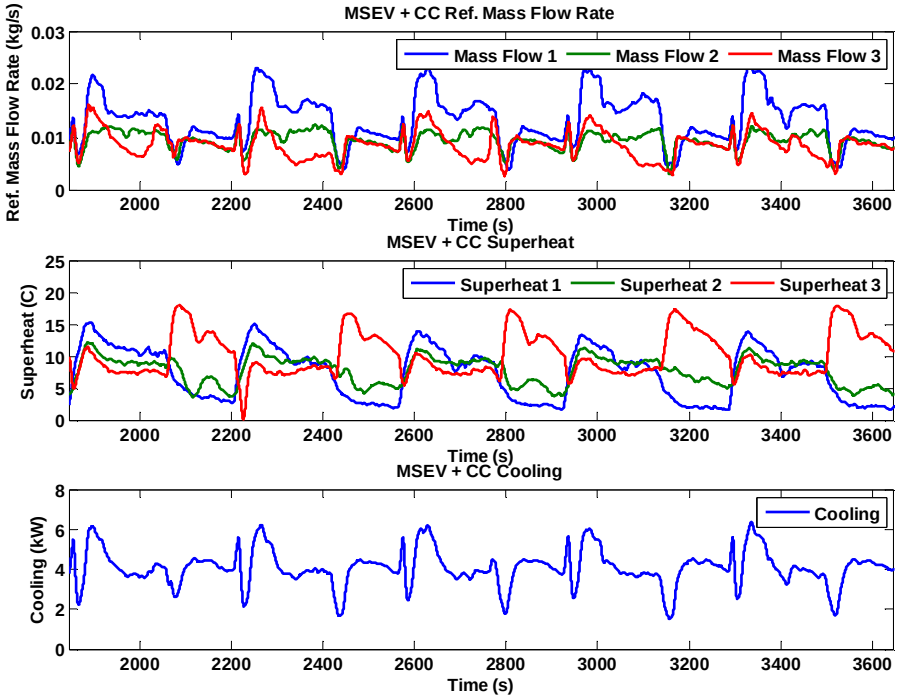

Figure 59: MSEVs with Cascaded Controller as a Comparison Group

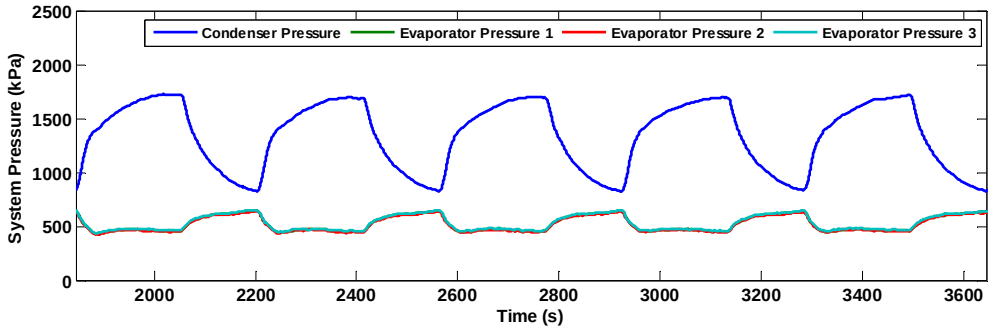

Figure 60: System Pressure - MSEVs with Cascaded Controller as a Comparison Group

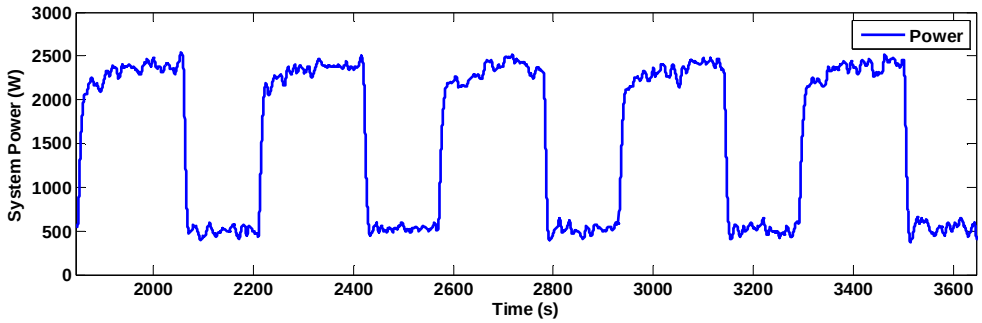

Figure 61: System Power Consumption - MSEVs with Cascaded Controller as a Comparison Group

As seen in Figure 62, Figure 63, Figure 64, Figure 65, average cooling, average superheat, system power consumption and cooling gained from the air side were compared in the cases above. The cascaded controller gained more average cooling than the cascaded controller with valve shut off. Average superheats of the three evaporators under these two control mechanisms were compared in Figure 63. From the plot, the average superheats were very similar in these testing conditions. Power consumptions by the whole system under these two control mechanisms were shown in Figure 64. As

seen in the plot, the power consumed during the on cycles was similar. But cycling time with cascaded controller was shorter than cascaded controller with valve shut off.

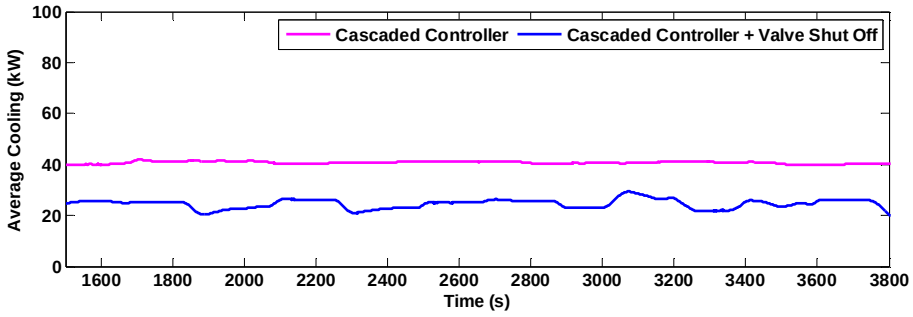

Figure 62: Average Cooling Per Cycle Comparison - Cascaded Controller vs. Cascaded Controller with Manual Valve Shut Off

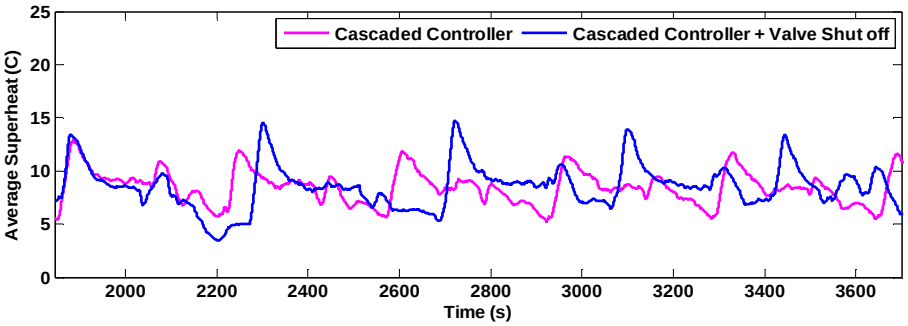

Figure 63: Average Superheat - Cascaded Controller vs. Cascaded Controller with Manual Valve Shut Off

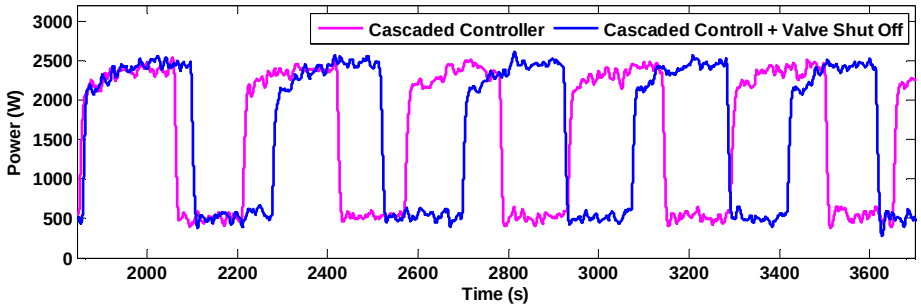

Figure 64: Power Consumption Comparison - Cascaded Controller vs. Cascaded Controller with Manual Valve Shut Off

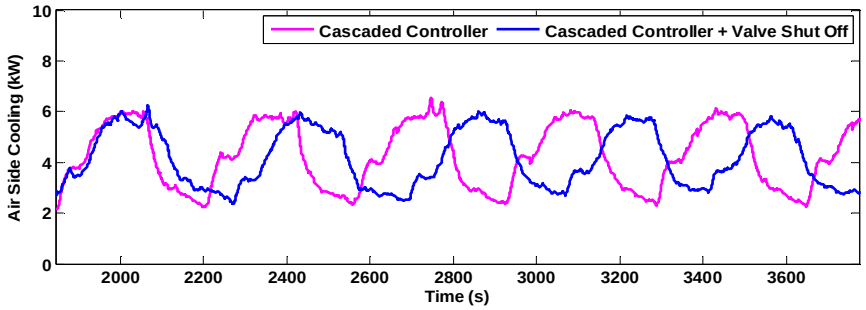

Figure 65: Air Side Cooling Comparison - Cascaded Controller vs. Cascaded Controller with Manual Valve Shut Off

Table 18: Numerical Comparison for Five Cycles - Cascaded Controller vs. Cascaded Controller with Manual Valve Shut off

	Power (kW)	Cooling Refrigerant (kW)	COP (Ref.)	Cooling Air (kW)	COP (Air)	Average Cycle Time (s)	Average Compressor On Time (s)	Average Compressor Off Time (s)
Cascaded Controller	15.7	40.9	2.6	42.5	2.7	360	210	150
Cascaded Controller + Valve Shut Off	15.8	24.4	1.5	41.8	2.6	386	224	166

In Table 18, numerical comparisons were given. Power consumption under the cascaded controller and the cascaded controller with manual valve shut off were similar. But running the system with only the cascaded controller, the system gained 67.6% more cooling from the refrigerant and a higher COP. The refrigerant side cooling is calculated based on the refrigerant mass flow rate which is not an appropriate way to calculate cooling when the compressor is off. The calculated refrigerant side cooling has a higher value due to the non-zero refrigerant mass flow rate during the off cycles. However, the air side did not gain that much cooling. So a better view is to compare the air side cooling. The cooling calculated from the air side is 42.5 KW using cascaded controller and 41.8 KW using cascaded controller with manual valve shut off. Average cycle time using cascaded controller is 360 seconds and 386 seconds using cascaded controller with manual valve shut off. Under the cascaded controller, the system has longer average compressor on - off time.

Numerical integration was used to calculate the area under the mass flow rate curve under the cascaded controller condition. The amount of refrigerant mass that migrated during one off cycle is around 1.9kg which is almost the total system charging amount.

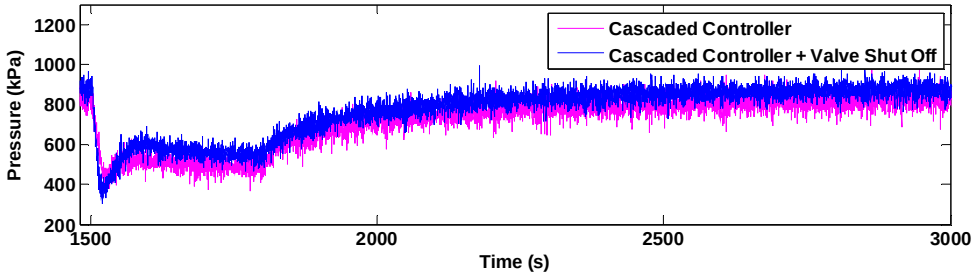

Figure 66: Evaporator Pressure Comparison - Cascaded Controller vs. Cascaded Controller with Manual Valve Shut Off

5.3 Fixed Time On-off Cycles (300 seconds on, 300 seconds off)

In this part of test, the system was set to the fixed time on-off cycles, 300 seconds on time and 300 seconds off time. The superheat set point was again 8°C. Five cycles of data were plotted under each control mechanism.

5.3.1 TXV

Figure 67 shows 5 cycles' data of mass flow rate, superheat and cooling when the system was running with TXVs. Superheats were stabilized to 10°C during compressor on cycles. Due to the evaporator fans were being left on after the compressor shutdown, the refrigerant in the evaporators boiled and resulted in non-zero superheat.

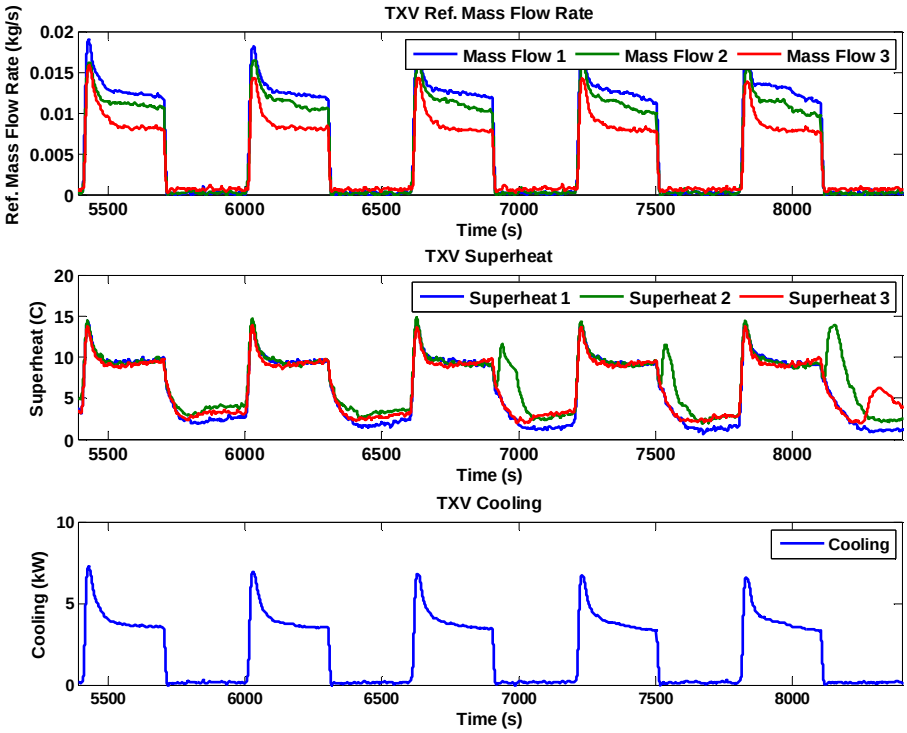

Figure 67: System Parameters with TXVs - Case 2

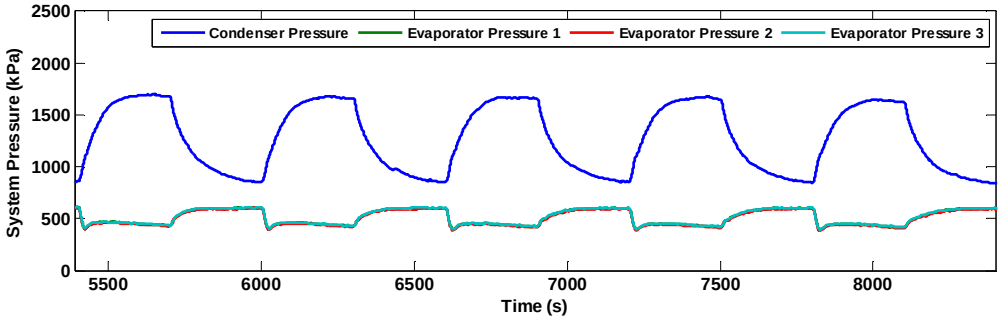

Figure 68: System Pressure with TXVs - Case 2

5.3.2 MSEV + USHC

Figure 69 shows the system parameters when the system was running with MSEVs and USHCs. From the superheat plot, we can see the USHC cannot bring the superheat down to 8 °C in 300 seconds.

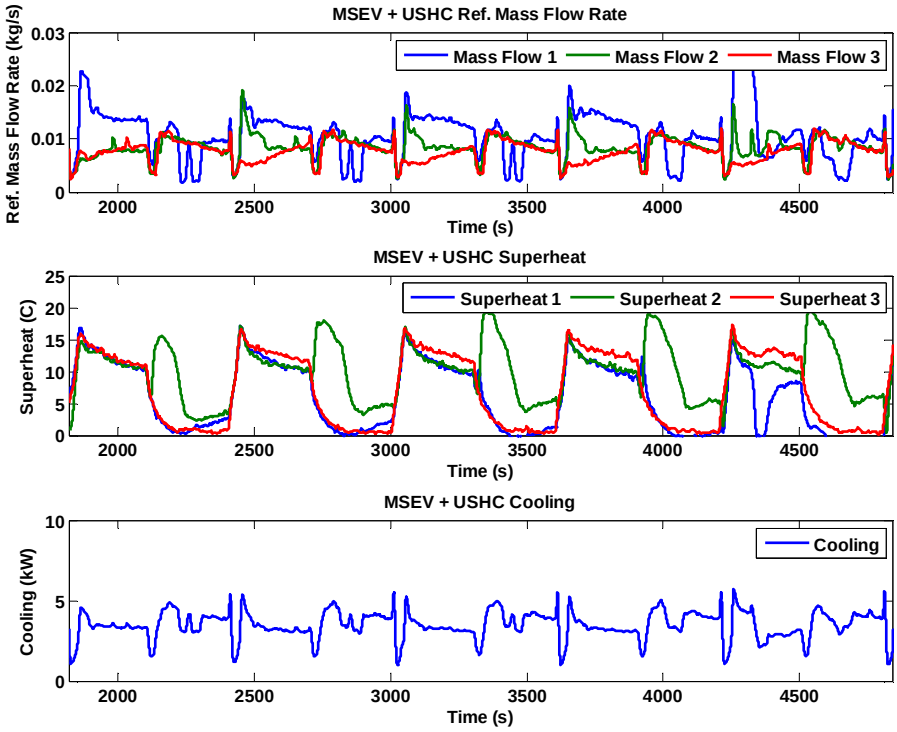

Figure 69: System Parameters with MSEVs and USHC - Case 2

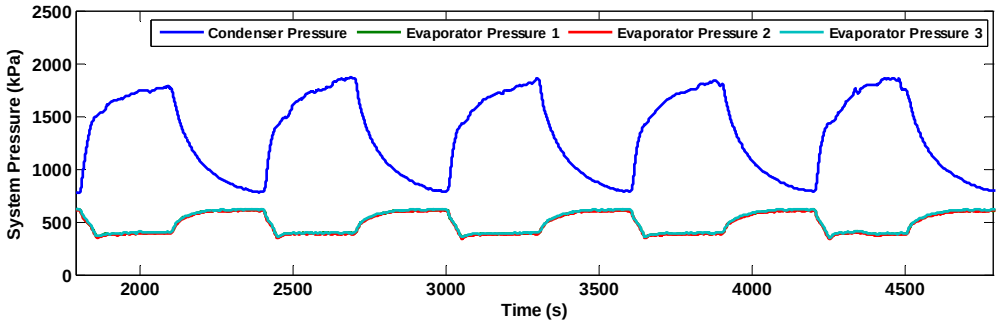

Figure 70: System Pressure with MSEVs and USHC - Case 2

5.3.3 Cascaded Controller

A cascaded controller was applied on the MSEVs. The superheat set point was 8 °C. In Figure 71, refrigerant mass flow, superheat and cooling were plotted. Superheat 2 and 3 were related to 8 °C. Superheat 1 was settled to 10 °C. During the compressor off cycles, the superheat did not reach to zero. This is because the evaporator fans were left running and continued boiling refrigerant.

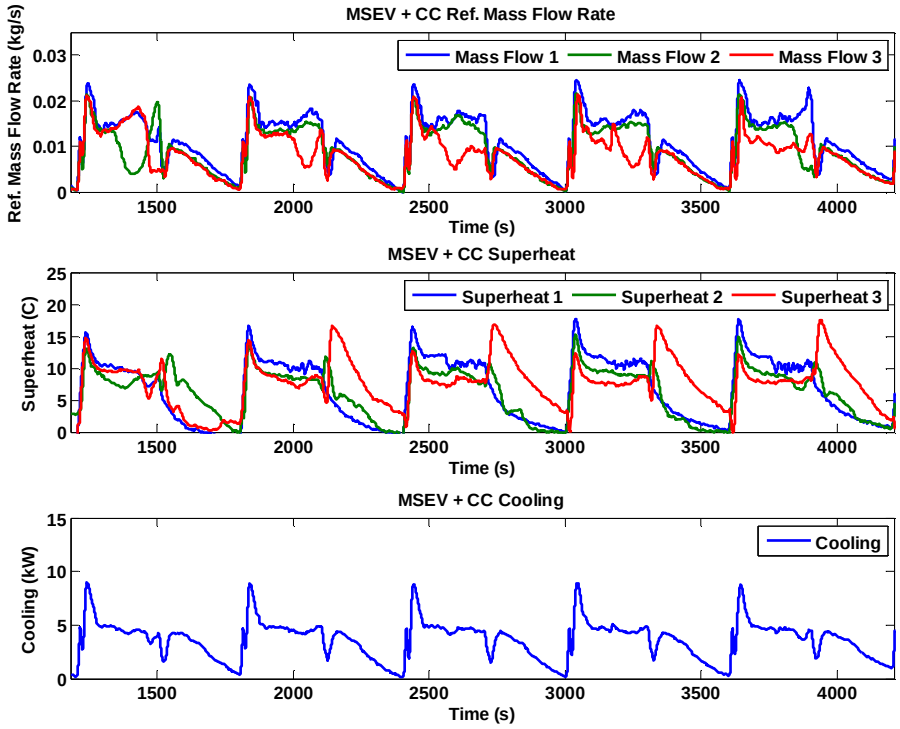

Figure 71: System Parameters with MSEVs and Cascaded Controller - Case 2

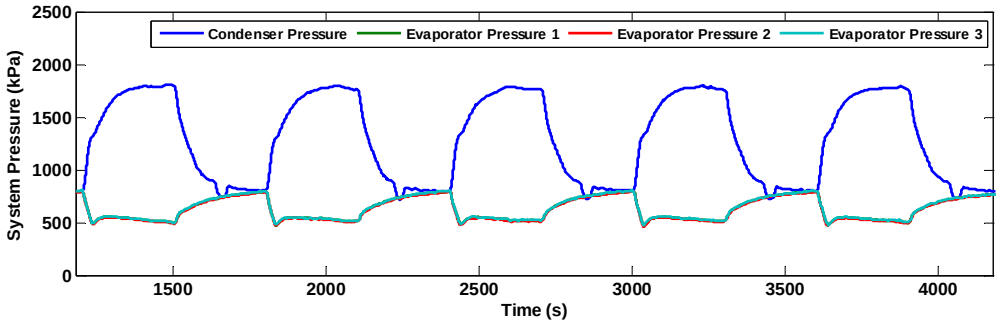

Figure 72: System Pressure with MSEVs and Cascaded Controller - Case 2

5.3.4 Cascaded Controller + Manual Valve Shut Off

The same cascaded controller mentioned earlier was applied to the MSEVs. The ball valves before the MSEVs were manually shut off when the compressor shut off and manually opened when the compressor started. Refrigerant mass flow rate, superheat and cooling were shown in Figure 73. The refrigerant mass flow was cut to zero due to the closing of the ball valves during the off cycles. But the superheat remained positive because evaporator fans were left on during the off cycles.

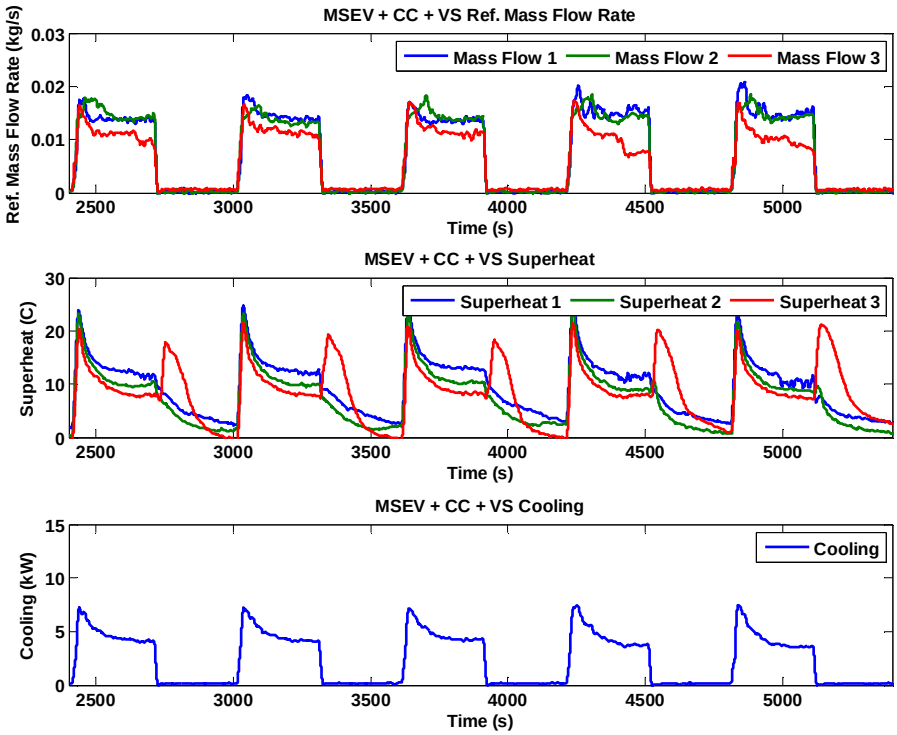

Figure 73: System Parameters with MSEVs and Cascaded Controller and Manual Valve Shut off - Case 2

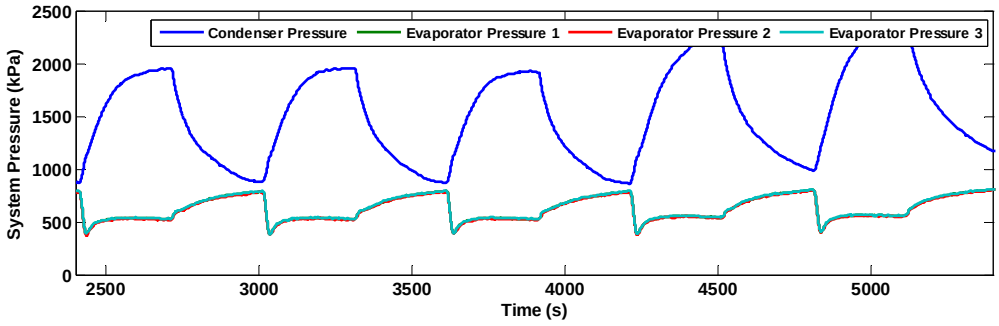

Figure 74: System Pressures with MSEVs and Cascaded Controller and Manual Valve Shut off - Case 2

5.3.5 Cascaded Controller + Valve Shut Off + Water Valve Shut Off

In this part of test, another element, a condenser water valve, was involved. During the test, the condenser water inlet valve was controlled by the compressor on and off signal. When the compressor was turned off, the off signal was sent by the computer to the condenser water valve. When the compressor was turned back on, the condenser water valve was opened by the control signal. Superheat set point was 8 °C. All the crucial system parameters were shown in Figure 75.

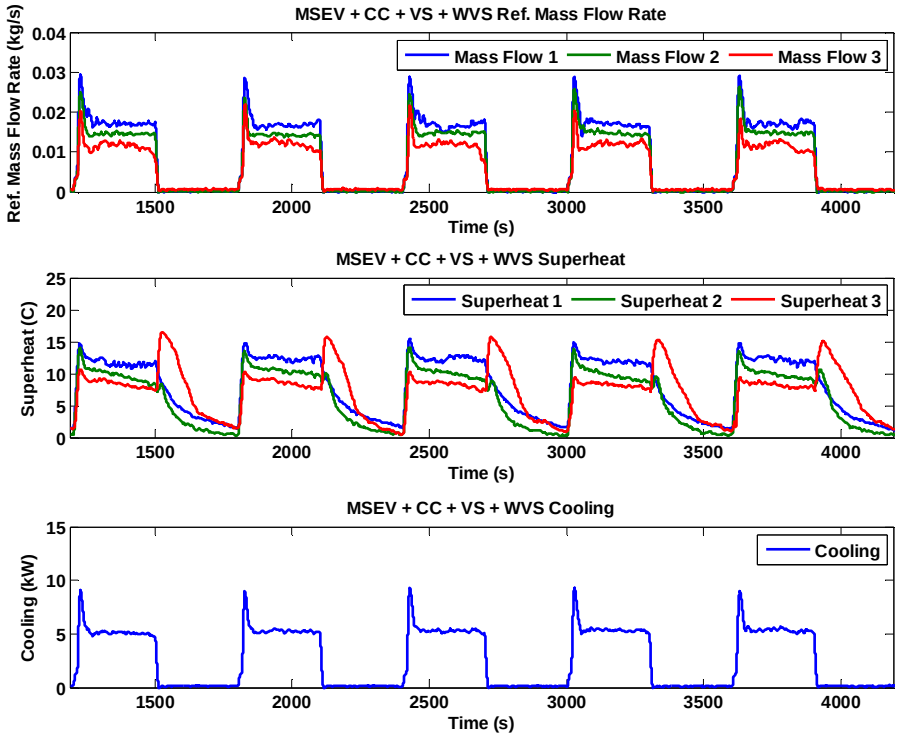

Figure 75: System Parameters with MSEVs and Cascaded Controller and Manual Valve Shut Off and Condenser Water Valve Shut off - Case 2

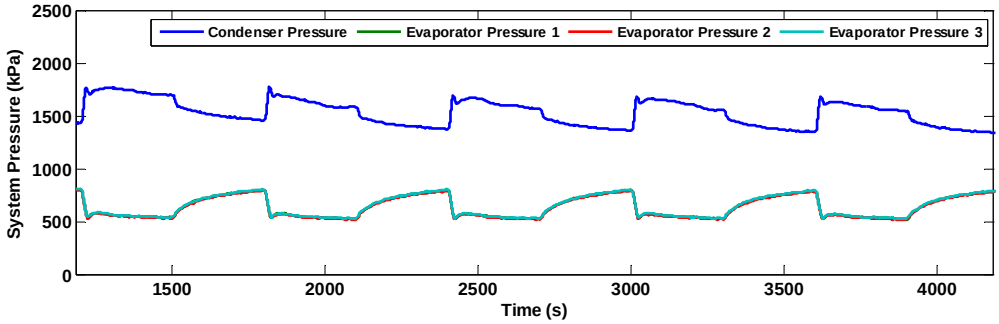

Figure 76: System Pressure with MSEVs and Cascaded Controller and Manual Valve Shut Off and Condenser Water Valve Shut off - Case 2

Summarizing 5 test configurations above in case 2, we have the following results. In Figure 77, total cooling calculated from refrigerant from 5 test configurations were plotted together. A 300 seconds moving average of cooling per cycle was plotted in Figure 78. Cascaded control without the valve shut off has the most amount of cooling; because there is a large amount of cooling during the off cycle. Compared to TXV, USHC gained 70.05% more cooling and 66.67% COP improvement. Cascaded control has 77% more cooling compared to TXV and 66.67% COP improvement. Cascaded control with manual valve shut off and cascaded controller with manual valve shut off and condenser water valve shut off did not show efficiency improvement as expected. Shutting off the expansion valve during the off cycle prevents the refrigerant migration and helps to build the pressure differential faster when the compressor starts again. But the superheat regulation in both valve shut off case and valve open cases are the same. The amount of cooling air gained is more or less the same. All the detailed data was listed in Table 19.

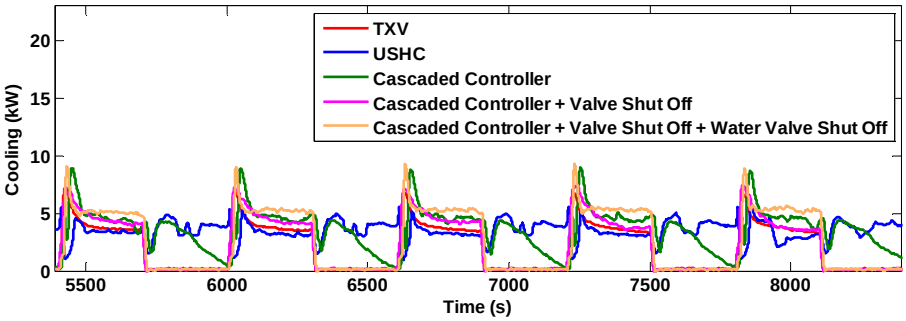

Figure 77: System Cooling - Case 2

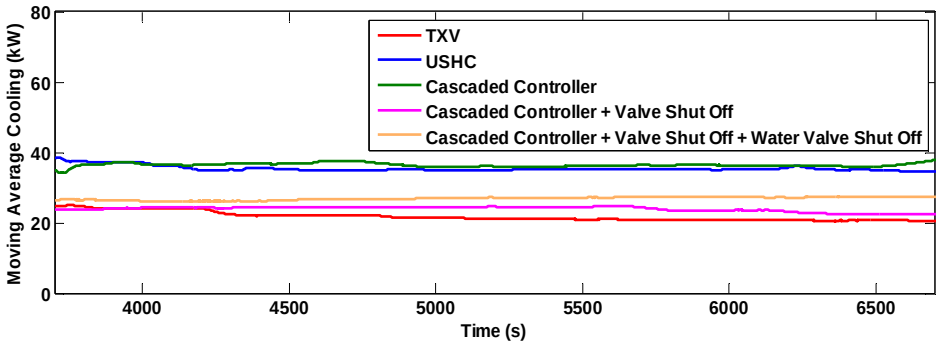

Figure 78: Average Cooling Per Cycle - Case 2

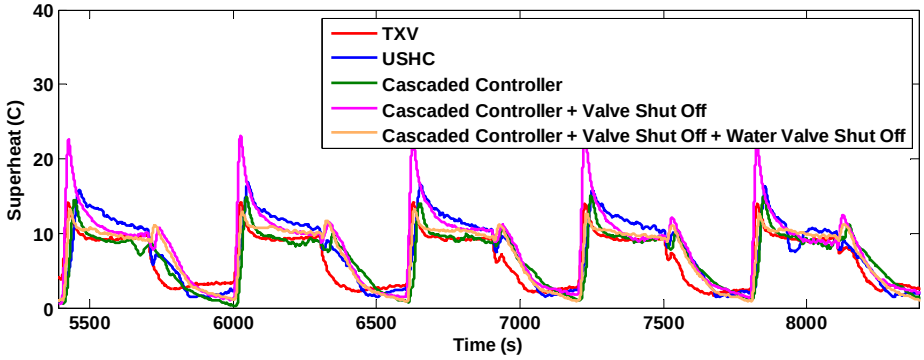

Figure 79: Average Superheat - Case 2

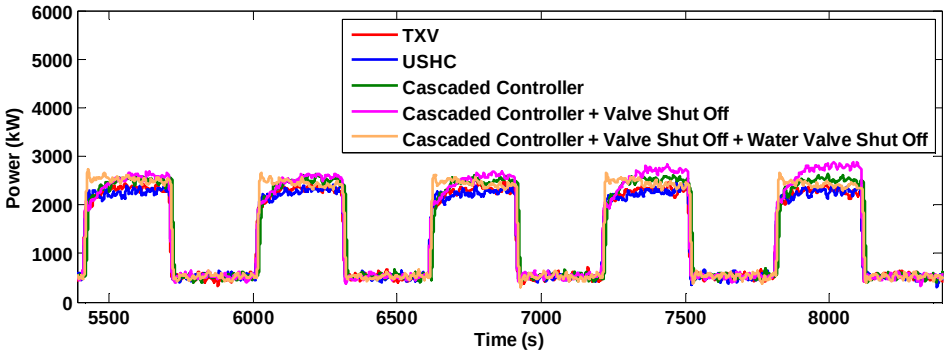

Figure 80: Power Consumption Comparison - Case 2

Table 19: Numerical Comparison for Five Cycles - Case 2

	Power (kW)	Cooling Air (kW)	COP Air	Cooling Ref. (kW)	COP Ref.
TXV	13.9	25.9	1.9	20.7	1.5
USHC	13.8	24.4	1.8	35.2	2.5
Cascaded Controller	14.8	36.4	2.5	36.64	2.5
Cascaded Controller + Valve Shut Off	15.19	35.8	2.4	23.85	1.6
Cascaded Controller + Valve Shut Off + Water Valve Shut Off	14.91	38.8	2.6	26.97	1.8

5.4 Fixed Time On-off Cycles (300 seconds on, 1200 seconds off)

In case 2 (fixed time compressor cycles, 300 seconds on and 300 seconds off), test configuration cascaded control with manual valve shut off didn't show efficiency improvement compared with cascaded controller as expected. In this part, the compressor off time during each cycle was extended to 1200 seconds. Three test configurations were conducted in this part, USHC, cascaded controller and cascaded controller with manual valve shut off. Superheat set point was 8 ℃.

In Figure 81, four cycles of data with MSEVs and USHC were shown. In the superheat plot, the measured superheat was a lot higher than the superheat set point 8 °C. Due to the longer compressor off time in each cycle, the mass flow rate went down to zero after the pressures equalized after approximately 180 seconds.

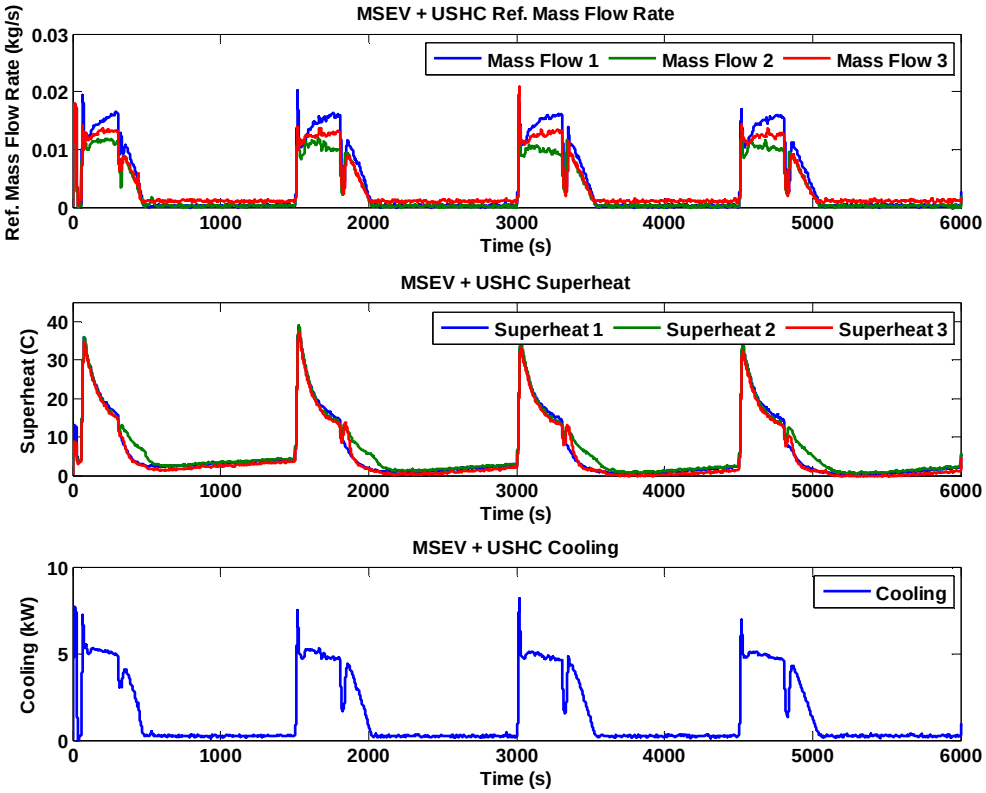

Figure 81: System Parameters with MSEVs and USHC - Case 3

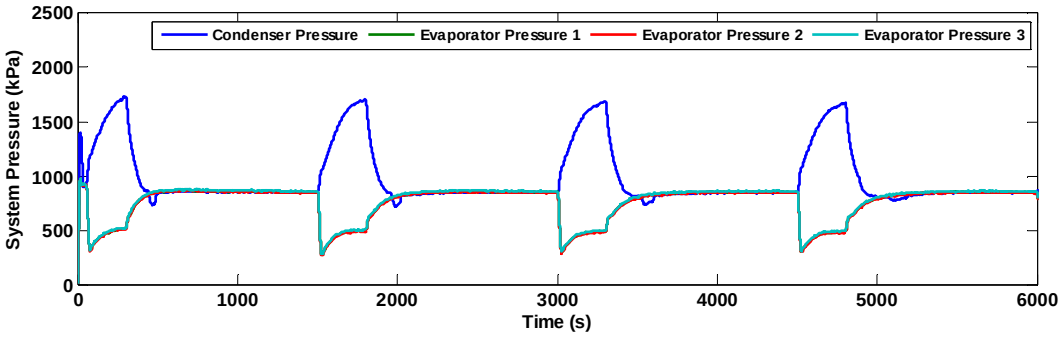

Figure 82: System Pressure with MSEVs and USHC - Case 3

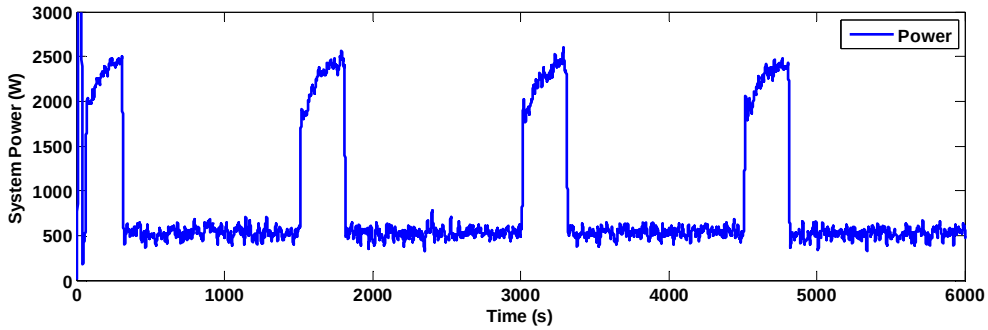

Figure 83: System Power Consumption with MSEVs and USHC - Case 3

In Figure 84, a cascaded controller was applied on the MSEVs. The measured superheat was still higher than the set point compared with USHC. A certain amount of cooling was gained during the off cycle due to open valve which allowed refrigerant going through when there was still a pressure difference across the MSEVs.

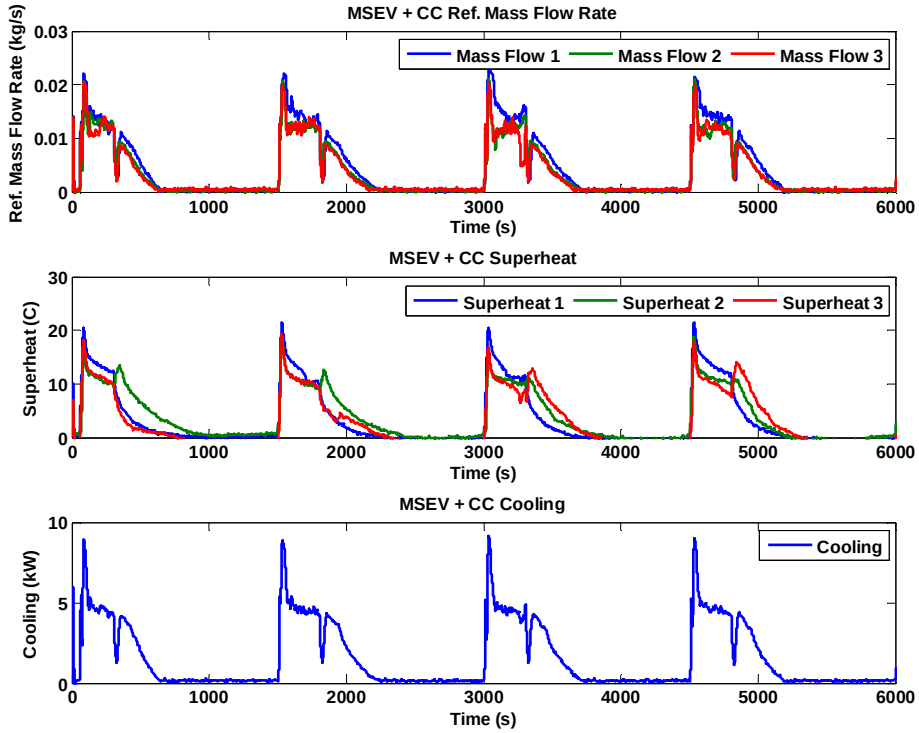

Figure 84: System Parameters with MSEVs and Cascaded Controller - Case 3

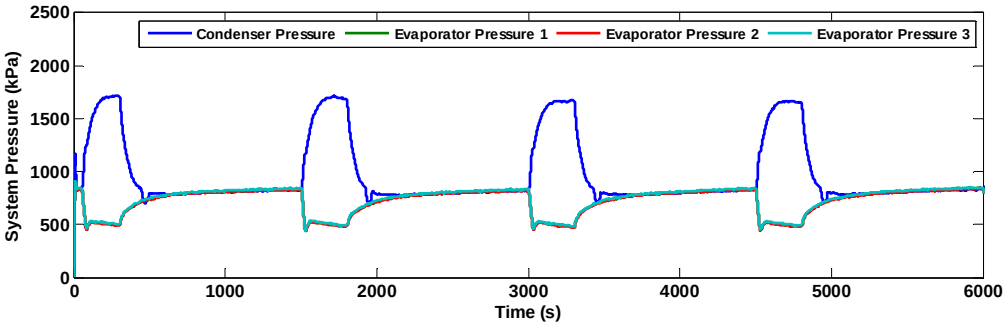

Figure 85: System Pressure with MSEVs and Cascaded Controller - Case 3

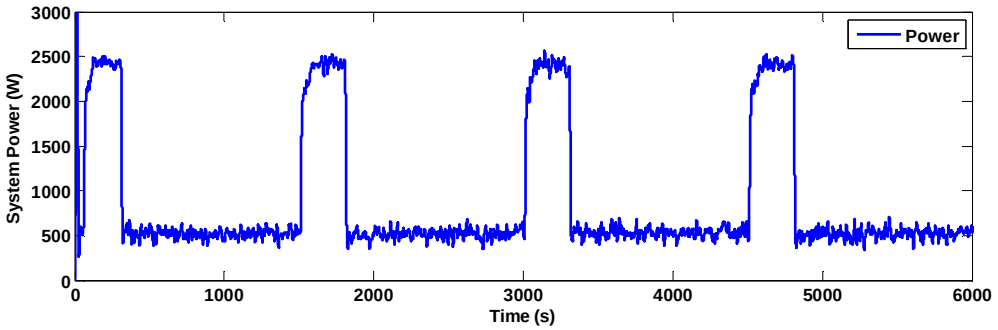

Figure 86: System Power Consumption with MSEVs and Cascaded Controller - Case 3

In Figure 87, a cascaded controller with manual shut off the ball valves before the MSEVs during off cycles was applied and there was no refrigerant migration. Therefore there was no mass flow and refrigerant migration during the compressor off cycle. The evaporator fans were kept running during the compressor off cycle which caused the refrigerant in the evaporator to boil leading to a non-zero superheat at the beginning of the off cycle. Given enough time, the superheat eventually equalized to zero.

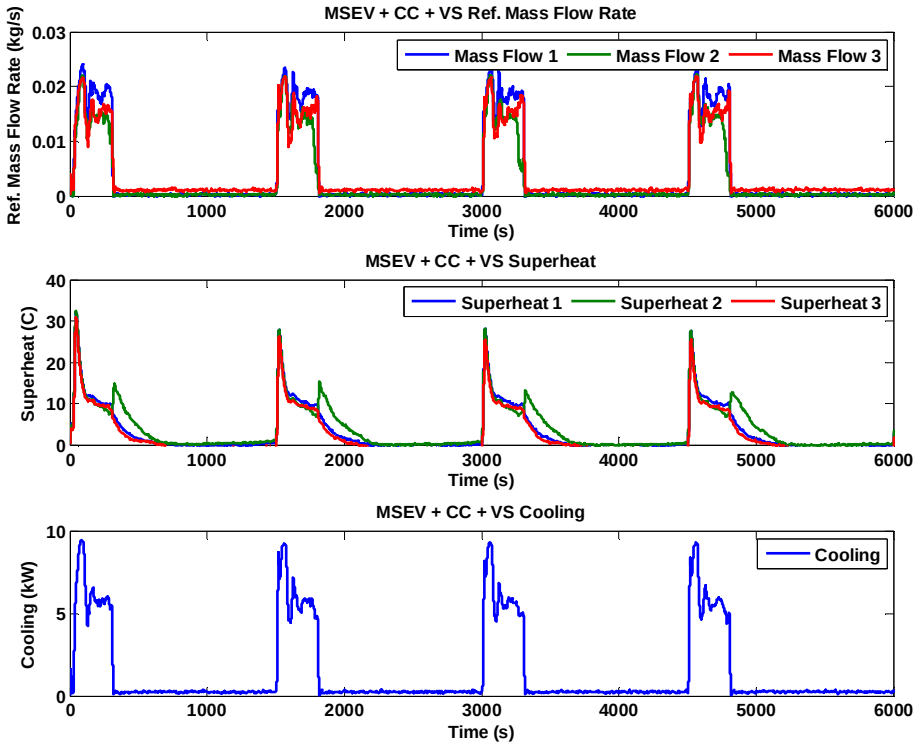

Figure 87: System Parameters with MSEVs and Cascaded Controller and Manual Valve Shut off - Case 3

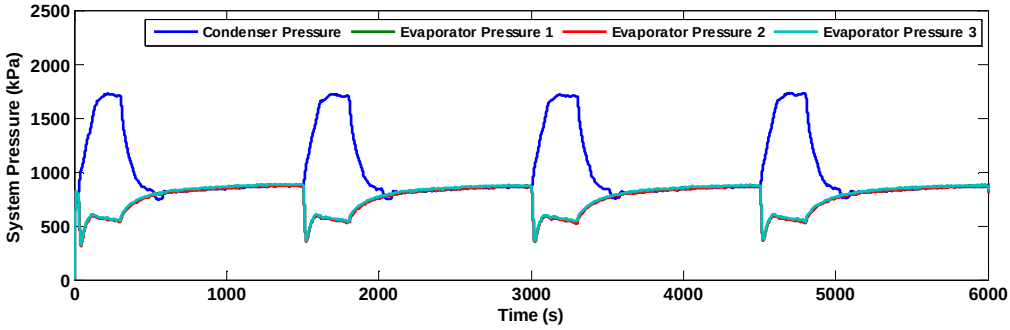

Figure 88: System Pressure with MSEVs and Cascaded Controller and Manual Valve Shut off - Case 3

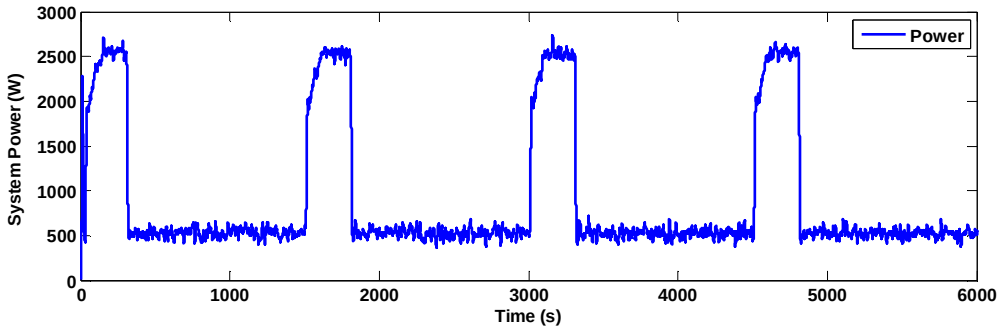

Figure 89: System Power Consumption with MSEVs and Cascaded Controller and Manual Valve Shut off - Case 3

In Figure 90, the average superheat of the three test configuration in case 3 was calculated and plotted. All the superheats in case 3 were higher than the superheat setpoint 8 °C, but they have the following order:

USHC > Cascaded controller > Cascaded Controller with manual valve shut off

In case 3, the compressor off time was longer than the other cases. Due to the longer off time, the case temperature warmed up during each cycle which gave the system a high temperature start point. It is obvious 300 seconds of compressor on time was enough for all these three control mechanisms to regulate the superheat to the set point.

In Figure 91, average cooling per cycle was calculated and plotted. Cascaded controller has the highest cooling per cycle followed by USHC, followed by cascaded control with manual valve shut off. This test result is the same as the case 2 test result.

From case 2 and case 3 test results, one can conclude that preventing refrigerant migration does not improve efficiency in refrigeration systems.

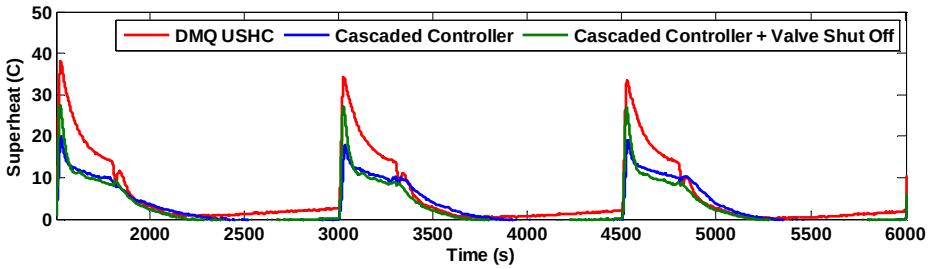

Figure 90: Average Superheat - Case 3

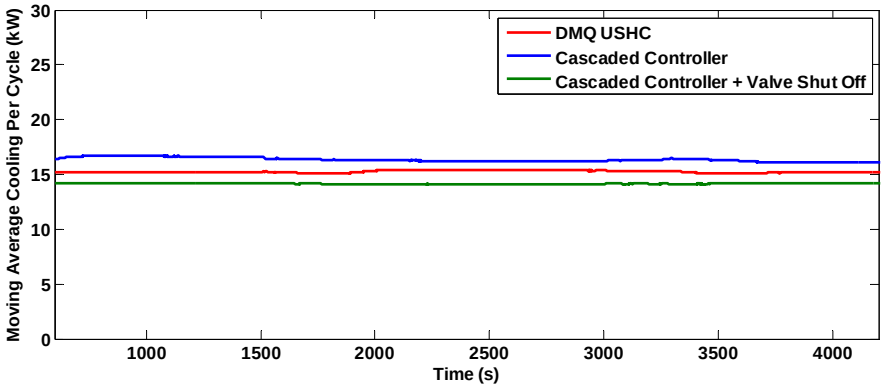

Figure 91: Moving Average Cooling Per Cycle - Case 3

Table 20: Numerical Comparison for Four Cycles - Case 3

	Power (kW)	Cooling Air (kW)	COP (Air)	Cooling Ref. (kW)	COP (Ref.)
DMQ USHC	8.7	14.2	1.6	15.3	1.8
Cascaded Controller	8.8	20.88	2.4	16.3	1.9
Cascaded Controller + Valve Shut Off	9.1	16.8	1.8	14.2	1.6

5.5 Low Temperature and Medium Temperature Comparison

Food products, fresh meats and produce, and stored items require strict environmental conditions for storage with a wide range of temperatures from -35 ℃ to 20 °C to provide the exact low temperature environment appropriate for each stored item, application, and scale of operation.

Having the simplicity of general-use air conditioners, medium temperature air conditioners deliver cool temperatures of 10 ℃ to 25 ℃. Beginning with food processing where a properly controlled environmental is essential to product freshness, applications include year-round cooling of IT rooms, constant temperature of precision equipment rooms and laboratories, and optimum temperatures of greenhouses.

In this part of tests, both of the cascaded controllers and DMQ's USHC were tested in both low temperature and medium temperature conditions. In the low temperature case, the system switch temperature on is -1.1 ℃ and system switch off temperature is 0 ℃. 16 ℃ is set as the switch on temperature and 11 ℃ as the switch off temperature in the medium temperature case. In these two cases, the superheat set point is 8 °C.

In the part, the cascaded controller is well tuned. The inner loop that determines the valve opening position was first tuned. Once the system has the ability to reach a stable operating condition, the outer loop was added to the controller. Based on the stable performance, the outer loop gains were added to the controller. The combination of the outer loop and inner loop gives the cascaded controller the ability to handle system disturbance.

5.5.1 Low Temperature

In Figure 92, refrigerant mass flow rate, superheat and cooling data for five cycles using MSEVs with cascaded controller were plotted. Figure 93 shows the data of MSEVs with USHC. The average superheat in both of the tests were calculated and plotted in Figure 94. USHC shows a much higher superheat than the cascaded controller which results in the cascaded controller having a higher COP as seen in Table 21.

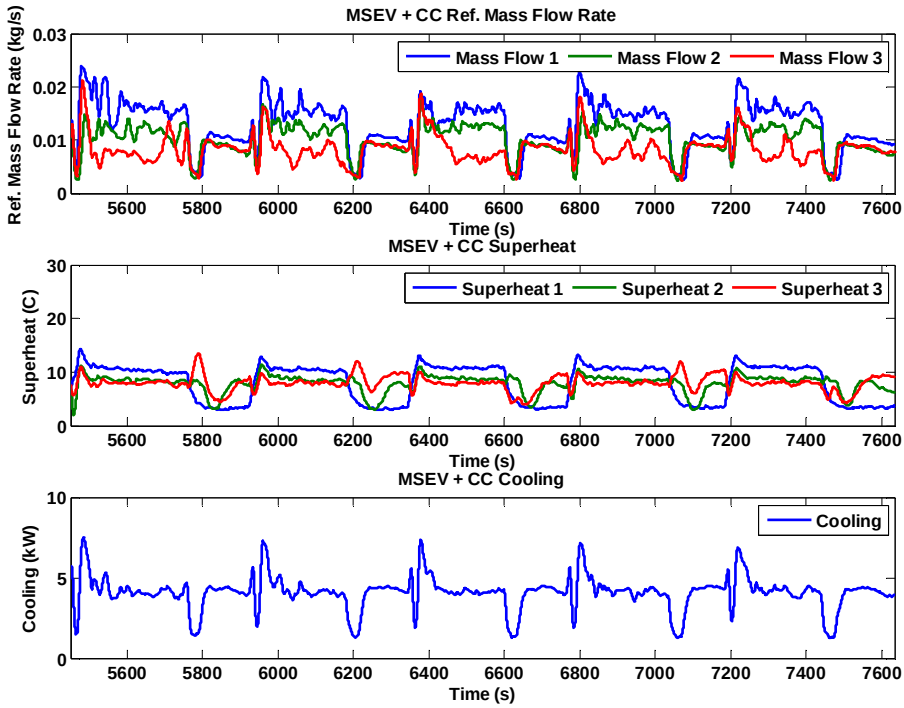

Figure 92: MSEVs with Cascaded Controller in Low Temperature Case

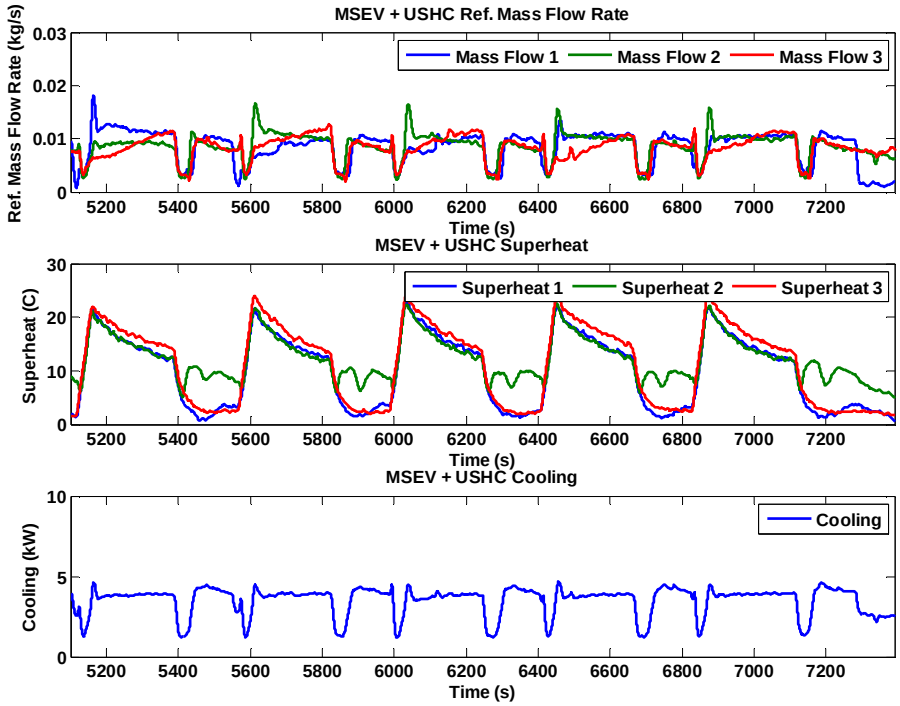

Figure 93: MSEVs with USHC in Low Temperature Case

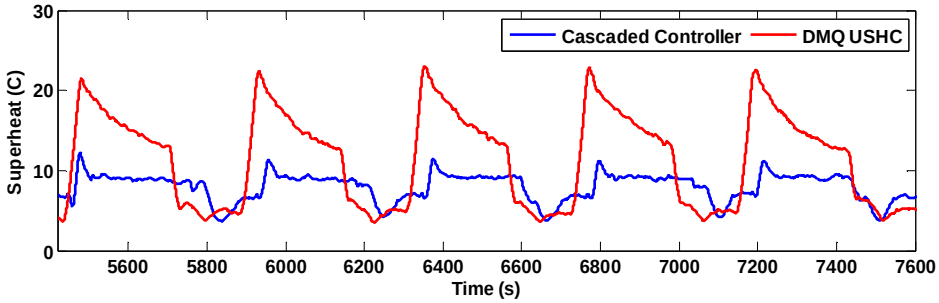

Figure 94: Average Superheat Comparison in Low Temperature Case

Table 21: Numeric Results in Low Temperature Case

	Power (kW)	Cooling Air (kW)	COP (Air)	Cooling Ref. (kW)	COP (Ref.)	Average Cycle Time (s)
DMQ USHC	14.19	27.09	1.9	35.27	2.5	450
Cascaded Controller	16.33	34.74	2.1	40.81	2.5	436

5.5.2 Medium Temperature

In Figure 95 and Figure 96, MSEVs with cascaded control and MSEVs with USHC in a medium case temperature were plotted. 16 °C is set as the switch on temperature and 11 °C as the switch off temperature in this case. Average superheats in both test configurations were shown in Figure 97. The results show that a cascaded controller has a lower superheat and higher total cooling. Numerical results are listed in Table 22.

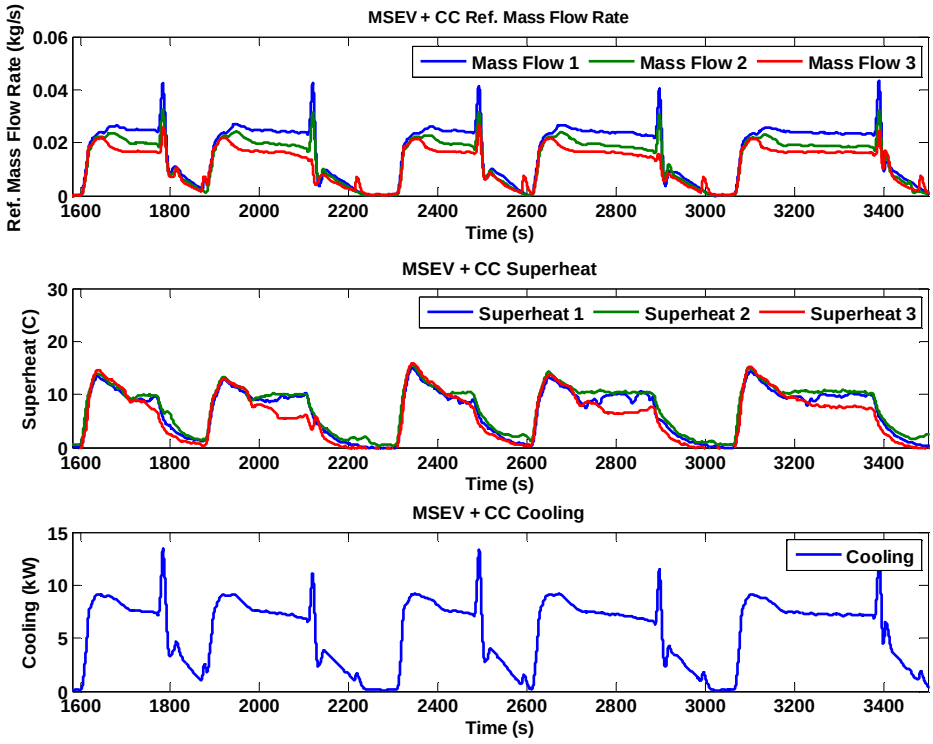

Figure 95: MSEVs with Cascaded Controller in Medium Temperature Case

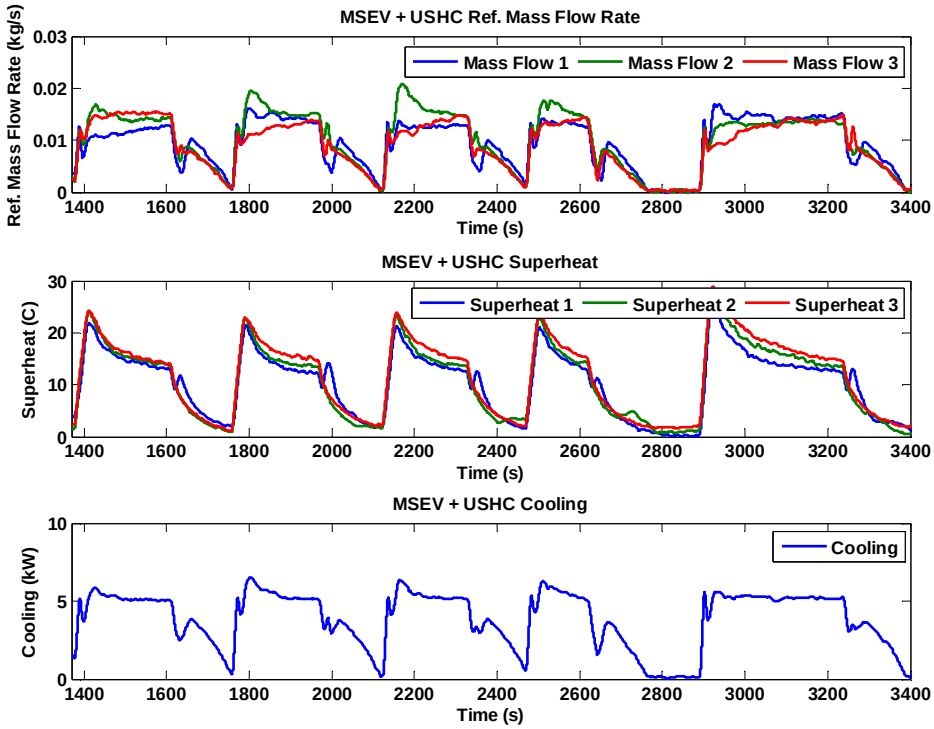

Figure 96: MSEVs with USHC in Medium Temperature Case

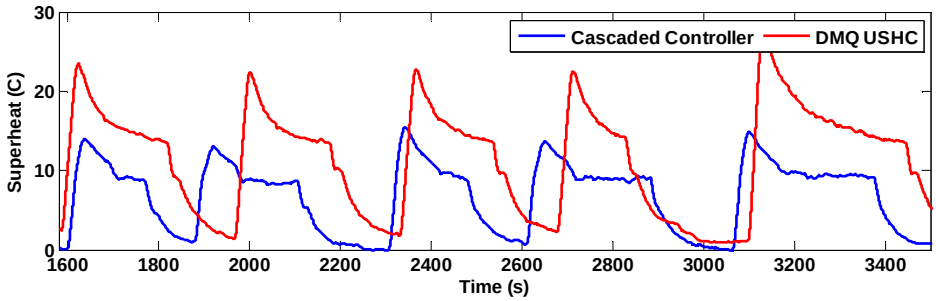

Figure 97: Average Superheat Comparison in Medium Temperature Case

Table 22: Numeric Results in Medium Temperature Case

	Power (kW)	Cooling Air (kW)	COP (Air)	Cooling Ref. (kW)	COP (Ref.)	Average Cycle Time (s)
DMQ USHC	15.24	47.44	3.1	38.24	2.5	412
Cascaded Controller	16.78	54.63	3.3	56.65	3.4	384

In these test cases, the results show that the cascaded controller works better than USHC in either low temperature case or medium temperature case. Once the cascaded controller is well tuned, it can handle both low case temperature and medium case temperature. The two-loop structure of the cascaded controller gives the system the ability to handle outside disturbance. In the medium temperature case, when the case temperature is higher, the outside loop can still regulate the pressure to the setpoint and the fast inner loop can regulate the superheat to the desired level.

5.6 Simulation of Refrigerant Migration

From the experimental results, a better view of valve shut-off technology of the off cycle is needed. Therefore a simulation of comparisons between expansion valve open during off cycle and expansion valve closed during off cycle is created. In this simulation, the model is simplified as a refrigeration system with one large evaporator [29]. The expansion valve used in the simulation is a TEV model. With a normal TEV, the valve is closed during the off cycle. For the valve open condition, the bulb pressure of the TEV is forced to a certain valve so that the TEV could stay partially open during the off cycle.

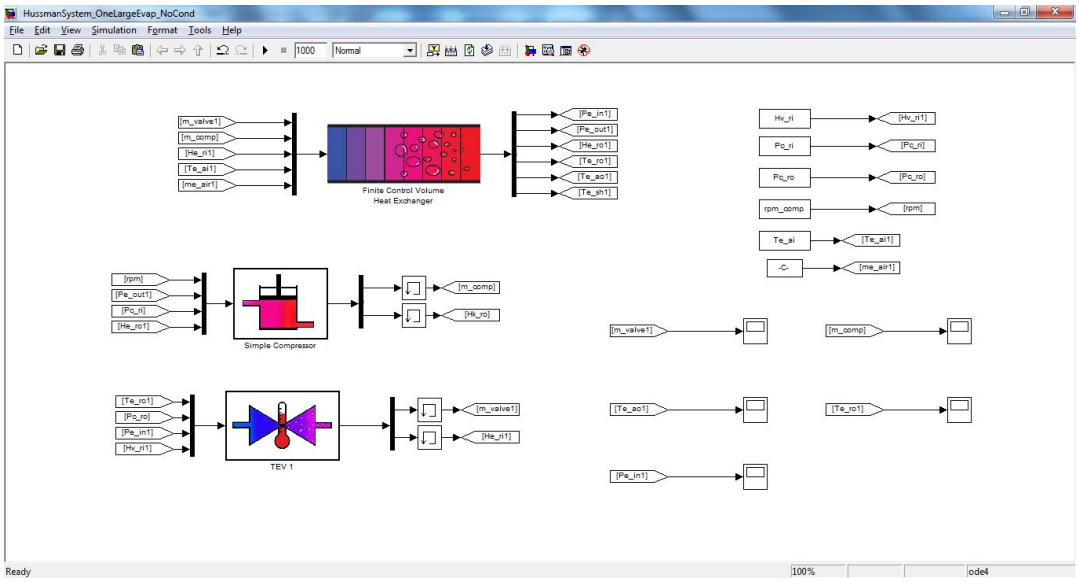

Figure 98: Schematic of the Simulation

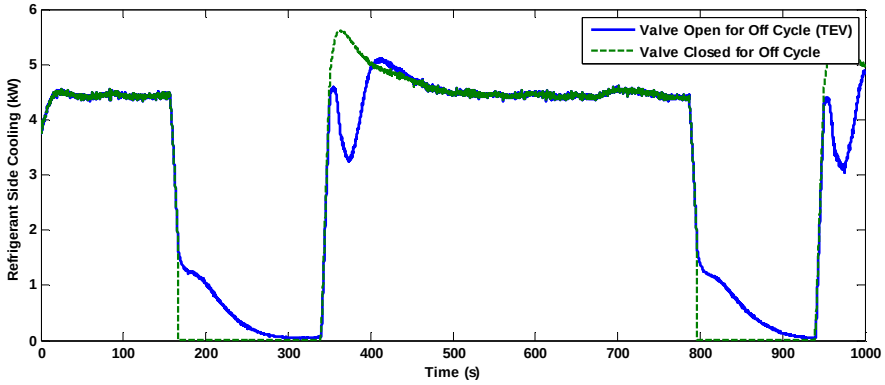

Figure 99: Refrigerant Side Cooling

From Figure 99, a certain amount of cooling was gained during the off cycle for the valve open condition. The total cooling from the refrigerant side is similar.

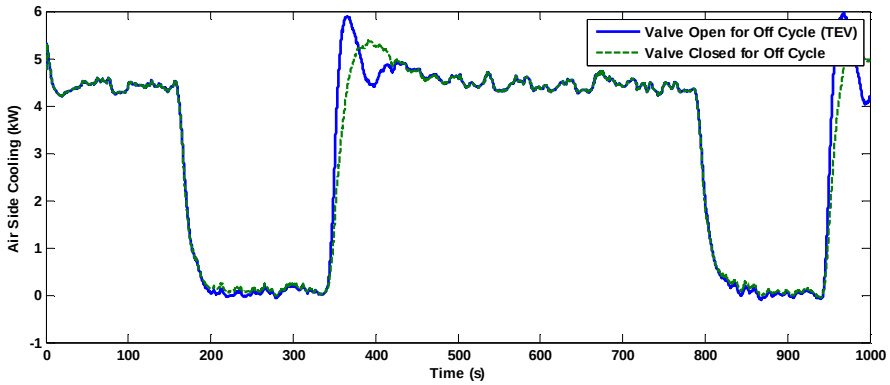

Figure 100: Air Side Cooling

Air side cooling is plotted in Figure 100. From this figure, we can see the total cooling from the air side is also very similar.

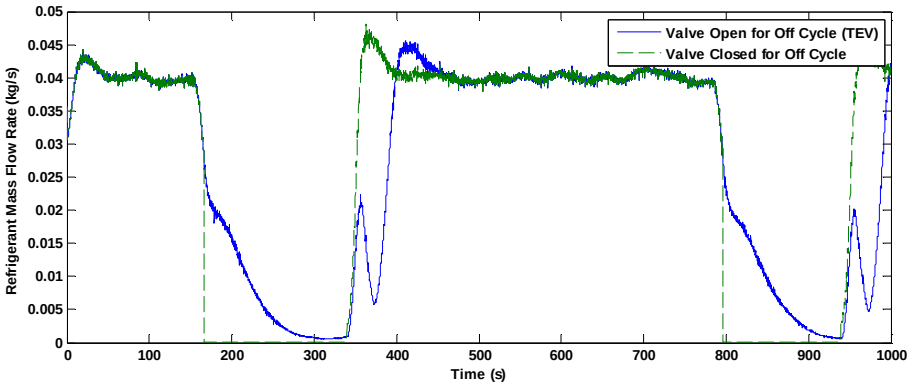

Figure 101: Refrigerant Mass Flow Rate

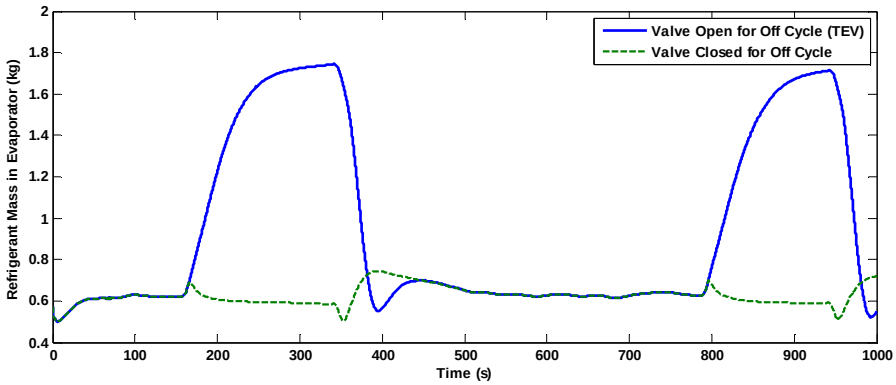

Figure 102: Refrigerant Mass in Evaporator

Refrigerant mass flow rate was plotted in Figure 101. In Figure 102, the refrigerant mass in the evaporator was plotted. For the valve open condition, during the off cycle, most of the refrigerant was stored in the evaporator. For the valve closed condition, the refrigerant mass in the evaporator did not vary significantly during the whole process.

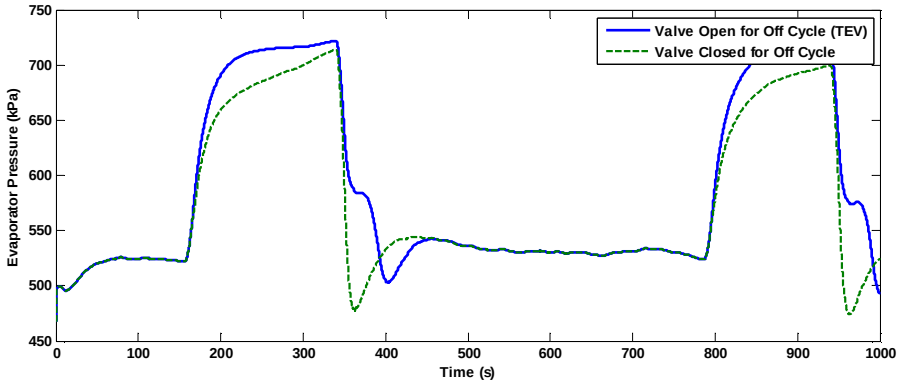

Figure 103: Evaporator Pressure

Evaporator pressure was plotted in Figure 103, which shows that for where the valve closed condition has a faster pressure pull down than the valve open condition. The operation pressure when the compressor was on for both the valve open condition and valve closed condition is the same.

5.7 Conclusion

From both the experimental results and the simulation results, the following conclusions can be made. DMQ's MSEV (Modular Silicon Expansion Valve) showed great advantages compared with traditional TXV (Thermal Expansion Valve). The cascaded controller showed the ability to handle the superheat in any condition and gained the most amount of cooling. Test cases using DMQ's USHC (universal superheat controller) also reveals the ability to maintain the superheat. But the gains of the USHC need to be tuned for each condition to have the best performance. Valve shut off technology does not show significant efficiency improvement as expected. Although using the valve shut off technology can prevent refrigerant migration during the off cycles and builds a pressure differential in the system more quickly, the total cooling gained from the air side does not show much difference.

CHAPTER VI

CONCLUSION AND FURTHER WORK

This project first experimentally examined the leakage rate and cooling capacity of DMQ's PDA valves on a multi-evaporator system. DMQ's PDAs showed relatively small leakage rate compared to traditional expansion valves. The examined valves showed a cooling capacity ranging from 77W to 380W which gives the PDAs the potential for application in refrigeration, air conditioning and electronics cooling.

A comprehensive set of experimental tests were conducted on the multi-evaporator Hussman refrigeration system to compare different control mechanisms under a variety of operating conditions. The expansion valves involved in this part of project was the MSEV (Modular Silicon Expansion Valve) manufacture by DMQ. The MSEV was compared with the traditional TXV (Thermal Expansion Valve) and showed large efficiency improvement. Different controller strategies were applied to the MSEVs. The cascaded controller and DMQ's USHC (universal superheat controller) both showed good performance, but the cascaded controller has the ability to control superheat across a wide range conditions. Valve shut off technology does not show a lot cooling gaining as expected. From the experimental results, Although using the expansion valve shut off technology can prevent refrigerant migration during off cycles and reduces loads associated with rebuilding the pressure difference across the system, the total cooling gained from the air side does not show much difference.

REFERENCES

[1] U.S. Building Energy Data Book, "U.S. Energy Consumption in 2011". Available at: http://buildingsdatabook.eren.doe.gov

[2] Ming Zhang, "Energy Analysis of Various Supermarket Refrigeration Systems", International Refrigeration and Air Conditioning Conference, p. 856, 2006.

[3] J. Michaels and A. Swenson, "Commercial buildings energy consumption survey—Overview of commercial buildings characteristics", 2003. Available: http://www.eia.gov/emeu/cbecs/cbecs2003/introduction.html [Accessed]

[4] M.S. Elliott and B. P. Rasmussen, "On reducing evaporator superheat nonlinearity with control architecture", International Journal of Refrigeration, vol. 33, issue 3, pp. 607-614, May 2010.

[5] B. P. Rasmussen, "Dynamic modeling for vapor compression systems—Part I: Literature review", HVAC&R Research, vol. 18, issue 5, pp. 934-955, 2012.

[6] M. S .Elliott, B. P. Rasmussen, Z. Bolding and B. Bolding, "Superheat control: A hybrid approach", HVAC&R Research, vol. 15, issue 6, pp. 1021-1043, November 2009.

[7] A. Henning, "Microfluidic MEMS", Aerospace Conference, 1988 IEEE, pp. 471-486.

[8] DunAn MicrostaqWebsite, "MEMS Microvalve Technology". Available at: http://www.dmq-us.com[Accessed]

[9] K. Higuchi, M. Hayano, “Dynamic Characteristics of Thermostatic Expansion Valves”, International Journal of Refrigeration, vol. 5, issue 4, pp. 216-220, July 1982.

[10] P. Mithraratne, N.E Wijeysundera, “An Experimental and Numerical Study of Hunting in Thermostatic-expansion-valve-controlled Evaporators”, International Journal of Refrigeration, vol. 25, issue 7, pp. 992-998, November 2002.

[11] N. J. Hewitt, J. T. McMullan, N. E. Murphy, C. T. Ng, “Comparison of Expansion Valve Performance”, International Journal of Energy Research, vol. 19, issue 4, pp.347-359, June 1995.

[12] B. P. Rasmussen, “Project Report-Technology Evaluation: Silicon Expansion Valve Potential Application and Advantages”, January 2009.

[13] Broersen, P.M.T. and van der Jagt, M.F.G., “Hunting of Evaporators Controlled by a Thermostatic Expansion Valve”, ASME Journal of Dynamic Systems Measurement & Control 102(2), pp. 130-135, June 1980.

[14] Farzad, M. and O'Neal, D.L., “Influence of the expansion device on air-conditioner system performance characteristics under a range of charging conditions”. ASHRAE Transactions 993-13. 1993.

[15] Choi, J.M. and Kim, Y.C., “The effects of improper refrigerant charge on the performance of a heat pump with an electronic expansion valve and capillary tube”. Energy 2002, vol. 27, issue 4, pp. 391-404. 2002.

[16] Xiang-Dong He, Sheng Liu. Harry H. Assada and Hiroyuki Itoh, "Multivariable Control of Vapor Compression Systems", HVAC&R Research, vol. 4, No. 3, pp.205-230, July 1998.

[17] L. S. Larsen, "Potential Energy Savings in Refrigeration Systems using Optimal Set-points", Proceedings of the 2004 IEEE International Conference on Control Applications, vol. 1, pp.701-704, September 2004.

[18] Changquin Tian, Chunpeng Dou, Xinjiang Yang and Xianting Li, "Instability of Automotive Air Conditioning System with Variable Displacement Compressor. Part 1. Experimental Investigation" , International Journal of Refrigeration, No.28, 2005.

[19] H. Rasmussen, "Nonlinear Superheat Control of a Refrigeration Plant using Backstepping", Proceedings - 34th Annual Conference of the IEEE Industrial Electronics Society, IECON 2008, pp. 286-290, 2008.

[20] H. Rasmussen, L. F.S. Larsen, "Energy Efficient Control of a Refrigeration Plant", 18th IEEE Conference on Control Applications, pp.1495-1500, July 2009.

[21] A. Gupta, "Dynamic Modeling and Cascaded Control for A Multi-evaporator Supermarket Refrigeration System", Master of Science thesis, Texas A&M University, College Station, Texas. 2012.

[22] S. E. Shafiei, R. Izadi-Zamananbadi, H. Rasmussen and J. Stoustrup, "A Decentralized Control Method for Direct Smart Grid Control of Refrigeration Systems", 52nd IEEE Conference on Decision and Control, pp. 6934-6939, December, 2013, Florence, Italy.

[23] M. S .Elliott, B. P. Rasmussen, “Decentralized Model Predictive Control of a Multi-evaporator Air Conditioning System”, Control Engineering Practice, vol. 21, issue 12, pp. 1665-1677, December 2013.

[24] Qureshi, T.Q. and Tassou, S.A., “Variable-Speed Capacity Control in Refrigeration Systems”. Applied Thermal Engineering, vol. 16, issue 2, pp. 103-113, February 1996.

[25] Gruhle, W.D. and Isermann, R., 1985. “Modeling and Control of a Refrigerant Evaporator”, American Control Conference 1985, pp. 287-292, June 1985.

[26] Outtagarts, A., Haberschill, P., and Lallemand, M., “ TheTransient Response of an Evaporator Fed through an Electronic Expansion Valve”, International Journal of Energy Research, vol. 21, issue 9, pp. 793-807, July 1997.

[27] Finn, D.P. and Doyle, C.J., “Control and Optimization Issues Associated with Algorithm-Controlled Refrigerant Throttling Devices”, ASHRAE Transactions 2000, vol. 106, part 1, pp. 524-533, July 2000.

[28] He, X.D., Asada, H., Liu, S., and Itoh, H., “Multivariable Control of Vapor Compression Systems”, HVAC&R Research, vol. 4, issue 3, pp. 205-230, July 1998.

[29] B. P. Rasmussen, “Dynamic modeling for vapor compression systems—Part II: Simulation tutorial”, HVAC&R Research, vol. 18, issue 5, pp. 956-973, February 2011.

APPENDIX

Leak test uncertainty calculation:

Pressure difference, ΔP, from condenser pressure P_1 to tank pressure P_2 is defined in equation (1).

$$\boldsymbol{\Delta P = P_1 - P_2} \tag{1}$$

$$\boldsymbol{\frac{d\Delta P}{dP_1} = 1}, \quad \boldsymbol{\frac{d\Delta P}{dP_2} = -1} \tag{2}$$

Uncertainty of pressure difference is given in equation (2):

$$\boldsymbol{u_{\Delta P} = \sqrt{\left[u_{P_1}\left(\frac{d\Delta P}{dP_1}\right)\right]^2 + \left[u_{P_2}\left(\frac{d\Delta P}{dP_2}\right)\right]^2} = \sqrt{\left(u_{P_1}\right)^2 + \left(u_{P_2}\right)^2}} \tag{3}$$

Where u_{P_1} is the uncertainty of condenser pressure sensor, $u_{P_2} = u_T \frac{dP}{dT}$ equals uncertainty of tank pressure and u_T is the uncertainty of temperature sensor

$\frac{dP}{dT} = \frac{dP_{sat}}{dT_{sat}}\Big|_{T=Tsat,measured}$ is calculated from NIST Reference Fluid Properties Software.

Leak rate $\dot{m}_{leak}$ is defined in equation(4):

$$\boldsymbol{\dot{m}_{leak} = \frac{m_{tank}(t_2) - m_{tank}(t_1)}{t_2 - t_1}} \tag{4}$$

$\boldsymbol{m_{tank}}$ is the total weight of the tank. $\boldsymbol{t}$ represents the time during the tests.

Uncertainty of leak rate calculation is shown in equation(5):

$$u_{\dot{m}_{leak}} = \sqrt{\begin{matrix}\left[u_{m_{tank}(t_2)}\left(\frac{d\dot{m}_{leak}}{dm_{m_{tank}(t_2)}}\right)\right]^2 + \\ \left[u_{m_{tank}(t_1)}\left(\frac{d\dot{m}_{leak}}{dm_{m_{tank}(t_1)}}\right)\right]^2 + \left[u_{t_2}\left(\frac{d\dot{m}_{leak}}{dt_2}\right)\right]^2 + \\ \left[u_{t_1}\left(\frac{d\dot{m}_{leak}}{dt_1}\right)\right]^2\end{matrix}} \tag{5}$$

$$\frac{d\dot{m}_{leak}}{dm_{tank}(t_2)} = \frac{1}{t_2 - t_1} \tag{6}$$

$$\frac{d\dot{m}_{leak}}{dm_{tank}(t_1)} = \frac{-1}{t_2 - t_1} \tag{7}$$

$$\frac{d\dot{m}_{leak}}{dt_1} = \frac{m_{tank}(t_2) - m_{tank}(t_1)}{(t_2 - t_1)^2} \tag{8}$$

$$\frac{d\dot{m}_{leak}}{dt_2} = -\frac{m_{tank}(t_2) - m_{tank}(t_1)}{(t_2 - t_1)^2} \tag{9}$$

$\boldsymbol{t}$ represents the time during the tests.

$u_{m_{tank}(t_1)}, u_{m_{tank}(t_2)}$ = uncertainty of mass measurement

u_{t_1}, u_{t_1} = uncertainty of time measurement

Cooling capacity test uncertainty calculation

Pressure difference from condenser pressure P_c to evaporator pressure P_e:

$$\boldsymbol{\Delta P = P_c - P_e} \tag{10}$$

$$\frac{d\Delta P}{dP_c} = 1 \tag{11}$$

$$\frac{d\Delta P}{dP_e} = -1 \tag{12}$$

Uncertainty of pressure difference:

$$u_{\Delta P} = \sqrt{\left(u_{P_e}\right)^2 + \left(u_{P_c}\right)^2} \tag{13}$$

u_{P_c}= uncertainty of condenser pressure sensor

u_{P_e}= uncertainty of evaporator pressure sensor

Valve cooling capacity:

Q is the cooling gained from the refrigerant. $\dot{m}$ represents the refrigerant mass flow rate. h_{outlet} is the enthalpy at the evaporator outlet. h_{inlet} is the enthalpy at the evaporator inlet. $u_{\dot{m}}$ is the uncertainty of mass flow measurement. $\frac{dh}{dP}, \frac{dh}{dT}$ are calculated from NIST Reference Fluid Properties Software.

$$Q = \dot{m}(h_{outlet} - h_{inlet}) \tag{14}$$

$$u_Q = \sqrt{\left[u_{\dot{m}}\left(\frac{dQ}{d\dot{m}}\right)\right]^2 + \left[u_{h_{outlet}}\left(\frac{dQ}{dh_{outlet}}\right)\right]^2 + \left[u_{h_{inlet}}\left(\frac{dQ}{dh_{inlet}}\right)\right]^2} \tag{15}$$

$$\frac{dQ}{d\dot{m}} = h_{outlet} - h_{inlet} \tag{16}$$

$$\frac{dQ}{dh_{outlet}} = \dot{m} \tag{17}$$

$$\frac{dQ}{dth_{inlet}} = -\dot{m} \tag{18}$$

$$u_{h_{outlet}} = \sqrt{\left[u_P\left(\frac{dh}{dP}|_{T=T_{eri},P=P_e}\right)\right]^2 + \left[u_T\left(\frac{dh}{dT}|_{T=T_{eri},P=P_e}\right)\right]^2} \tag{19}$$

$$u_{h_{inlet}} = \sqrt{\left[u_P\left(\frac{dh}{dP}|_{T=T_{cro},P=P_c}\right)\right]^2 + \left[u_T\left(\frac{dh}{dT}|_{T=T_{cro},P=P_c}\right)\right]^2} \tag{20}$$

Heat input from the heaters:

Q_h is the heat input from the heaters. V represents the voltage input to the heaters. I is the current input the heaters. u_V is the uncertainty of voltage measurement. u_I is the uncertainty of current measurement.

$$Q_h = V \times I \tag{21}$$

$$u_{Q_h} = \sqrt{\left[u_V\left(\frac{dQ_h}{dV}\right)\right]^2 + \left[u_I\left(\frac{dQ_h}{dI}\right)\right]^2} \tag{22}$$

$$\frac{dQ_h}{dV} = I \tag{23}$$

$$\frac{dQ_h}{dI} = V \tag{24}$$